Master's Thesis

Synthesis of fluorescent pNipam

Author:
Daan Verwijmeren

Supervisors:
Janne-Mieke Meijer
Andrei Petukhov

Van 't Hoff Laboratory for Physical and Colloid Chemistry
Debye Institute for Nanomaterials Science
Utrecht University

May 22, 2012

Abbreviations

AAc	acrylic acid
APS	ammonium persulfate
BIS	N'N-methylenebisacrylamide
DLS	dynamic light scattering
KPS	potassium persulfate
LCST	lower critical solution temperature
NBD	4-nitrobenzo[c][1,2,5]oxadiazole
NBD-MAEM	2-(methyl(7-nitrobenzo[c][1,2,5]oxadiazol-4-yl)amino)ethyl methacrylate
Nipam	N-isopropylacrylamide
pNipam	poly-N-isopropylacrylamide
SEM	scanning electron microscopy
SLS	static light scattering
TEA	triethylamine
TEM	transmission electron microscopy

Abstract

PNipam microgel particles display interesting behaviour due to their thermal response. The particles possess a lower critical solution temperature (LCST), which is 32 °C. Below the LCST, particles are water-soluble and therefore swollen with a large amount of water. Upon increasing the temperature above the LCST, water will be expelled from the particles interior, inducing shrinkage of the particle. This makes it possible to control the volume fraction of pNipam by changing the temperature. By mixing two of these pNipam systems of the same size at room temperature and at high volume fractions, mixed crystals can be obtained, which are interesting for defect studies. Since the LCST of a system can be altered by means of copolymerization, it is possible to induce shrinking or swelling to only one of the present systems. However, to conduct such an experiment, at least two distinct pNipam systems are needed. In this master thesis research, the synthesis of two suitable pNipam systems was the main goal. During this report an overview will be given of the synthesis results and the challenges that we came across in the search for suitable systems. In the end, we have been successful in preparations of dyed pNipam microgels under different reaction conditions and in copolymerization with AAc.

Contents

Chapter 1

Introduction

Many solid materials are crystalline, with their building blocks, for example atoms, ions and molecules, arranged into ordered repeating arrays extending in all three dimensions. Several properties of these materials arise from their crystallinity, such as strength, elasticity, electronic structure, etc. However, these properties are not present to an extent one would expect in a perfect crystal, because real crystals never have perfect crystalline ordering but contain defects.[1,2]

Defects are structural imperfections interrupting the ordering in a crystal. The presence of defects alters the behaviour of the material, and for example physically weakens strong crystalline materials. There are several categories of defects, such as point defects (0D), line defects (1D), plane defects (2D) and bulk defects (3D). A schematic 2D overview of a crystal is shown in figure 1.1, showing several defects: the absence of particles from the original material (vacancies); the presence of a particle of the original material on a non-lattice position (self-interstitial) or a linear discontinuity along one dimension (line defect). Furthermore, defects can also arise due to impurities, which lead to interstitial or substitution particles. Although defects can be disadvantageous (e.g. weakening the material), defects can also be added on purpose. It is known that the electronic behaviour of materials can be influenced by adding specific impurities, a process called doping.[3] Also, metals can be strengthened by work hardening, which is a process in which dislocations are induced.[2]

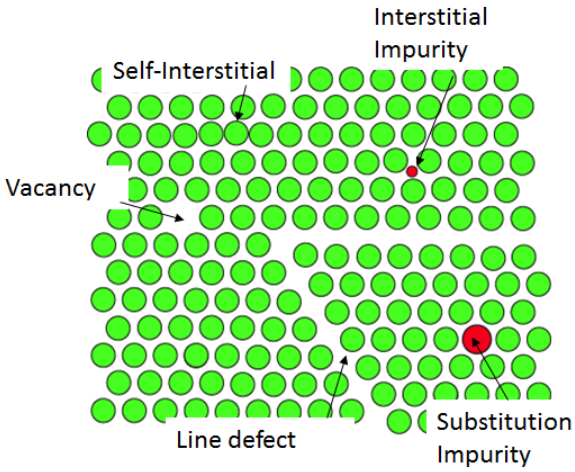

Figure 1.1: A schematic overview of a crystals and a few types of defects. Picture courtesy of Janne-Mieke Meijer.

Because crystals and their defects play an huge role in the behaviour of materials, a lot of research has been focussed on this topic. With more knowledge on crystals and defects, the properties of a material can be governed more easily. The effects of defects on the macroscopic properties of materials are well-described in many books.[1,2] However, studies on single particle and defect levels are still rare. Since atoms are small (typically 1 Å), so are the typical distances in an atomic crystal, as well as the typical dimensions of defects. For this reason, it is quite hard to observe single atoms and their crystals. Relatively complex techniques as x-ray scattering and high resolution electron microscopy have to be utilized to be conclusive about the behaviour of the materials defects. Furthermore, the time scale on

which atoms diffuse (nanoseconds), complicate matters even more.

Even though atomic defect studies on single defects are difficult to do, some researches have succeeded. An example is the research performed by Arakawa *et al.* at defects in iron foil.[4] Here, the researchers looked at the diffusion of dislocation loops in real time using TEM. Another notable example is the work of Matsukawa *et al.*[5] In this work, TEM was used to look at vacancy cluster migration in 1D in pure gold. Despite the high resolution, they still did not achieve single particle level resolution.

One way to overcome the size- and time scale problems, is the use of modelling techniques, like Lechner *et al.* did.[6] In their work, the diffusion of defects (interstitials and vacancies) was studied in a Monte Carlo simulation. In this research it was observed that the defects tend to aggregate in strings, which have a high mobility in 1D. This result was consistent with that of Arakawa *et al.* However, one ideally would want a model system in which crystalline behaviour and defects are present, with a higher observability of the building blocks. It is for this reason that in many studies, together with the one described in this thesis, colloids are used.

In physical chemistry "colloidal" is the name used for a system made up of particles between 1 and 1000 nm in size. Within this size range, particles show Brownian motion.[7] Furthermore, phase behaviour, similar to that of atoms and molecules, can be observed.[8] For these reasons, colloids are a popular and common model system for atoms. Also, colloids are much easier to study than atoms. Because atoms are only several Ångström at maximum, they cannot be observed with conventional light microscopy techniques. Colloids can be observed using microscopy techniques based on visible light. Moreover, the time scale on which colloids move is much higher, matching the time-resolution of common analysis equipment. Another advantage of colloids over atoms which should be noted, is the tunability of colloids. For many colloidal systems, small alterations during or after colloid synthesis can influence the properties of the colloids, like size, charge and shape. Furthermore, special properties like magnetic dipoles and chemical reactivity can be implemented. When all these factors are combined, it is possible to create a colloidal system in which the interactions at both short and long range are of the desired nature and magnitude.

The studies of colloids and their crystals and defects yield information which can be used to improve our knowledge about the behaviour of atoms and molecules. However, the information obtained in this way is also interesting on itself. Colloids have proven to be a promising way to produce photonic crystals.[9] For this reason, the information obtained by studying colloidal defects can also be translated to applications. Motivated by the above mentioned reasons, a lot of colloidal crystal and defect research has been performed.[8,10–12] Notable examples are the research by Pertsinidis *et al.* and Hilhorst *et al.*[13,14] Pertsinidis' research focusses on a 2D array of polysterene spheres. By introducing point defects with optical tweezers, they were able to watch the defects diffuse using optical microscopy. This way, single particle level movements could be observed. Hilhorst *et al.* looked at 3D crystals. Here, x-ray diffraction was used to study stacking faults in these crystals.[14]

In the examples of Pertsinidis and Hilhorst, the defects were induced in a 2D crystal, or the study was focused on intrinsic defects respectively. When one is able to induce defects *in situ* in a 3D crystal, very interesting studies can be conducted. With hard spheres this is difficult, since the only parameter in its phase behaviour is volume fraction, which cannot be easily changed *in situ*.

However, pNipam microgel particles offer an answer to this problem. In 1986, Pelton reported of the thermoresponsive behaviour of these particles. PNipam has a lower critical solution temperature (LCST) of 32 °C in water. Below this temperature the polymer dissolves in water and particles will be swollen. Above the LCST, the polymer is insoluble in water and the particles expel the water. In this way, the particles' volume can decrease up to 90 %.[15,16] In pNipam systems, the temperature change can be used as a tool to change volume fraction *in situ*. This property of the system has for example been used to induce melting at grain boundaries.[17,18].

In those cases, a system consisting of one type of pNipam was used. When a thermoresponsive pNipam system is mixed with a system with different properties, one can in principle induce shrinking or swelling to a part of the system. In this way it is possible to create vacancy-like, or interstitial-like defects respectively (as shown in figure 1.2). When the system consists of particles large enough (typically $d > 1.0\,\mu m$), visible light can be used to study the transitions in such a system. To achieve a high enough resolution and produce 3D reconstructions, confocal microscopy should be used. However, this adds another requirement on the particles, since the particles have to be fluorescent.

For the experiment mentioned above, two distinct systems are needed. Since the systems should have comparable refractive index and density, and no interactions, two pNipam systems will be used. The first being a pNipam system with a well-defined thermal response and the second having a different thermoresponsive behaviour. For this to work, one needs to alter the thermoresponsive behaviour of one

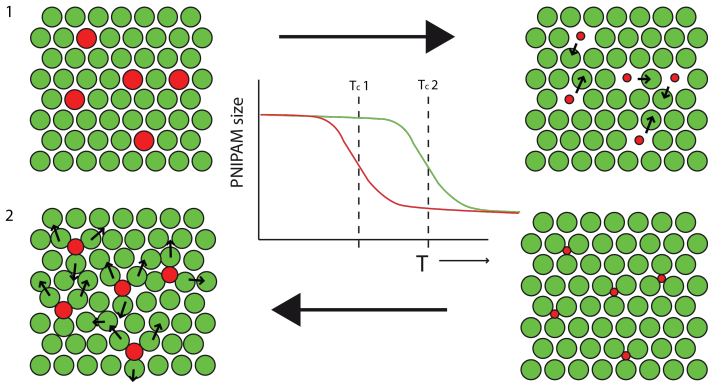

Figure 1.2: Schematical representation of two crystals of mixed fluorescent pNipam systems. The particles depicted by the green spheres has a relatively high LCST, whereas the other has a lower LCST. Top: The system starts in an equilibrated state at a temperature below both LCST's. Upon a slight increase in temperature, only the system depicted with red spheres will respond. Defects wil be introduced and the diffusion can be studied by confocal microscopy. Bottom: The system starts in an equilibrated state at a temperature in between both LCST's. Upon a decrease in temperature, the smaller system will swell again, creating stress in the crystal which will lead to movement.

of the systems. This can be achieved by the addition of comonomers which respond to other stimuli than temperature. For example, acrylic acid copolymerization introduces an pH response to the particles.[19] Summarized, all of the systems should have well defined stimuli-responsive behaviour, should be synthesized in a well-defined reproducible manner and exhibit sufficient fluorescence to make confocal studies possible. In this thesis the attempts of preparation of fluorescent pNipam microgel particles are described.

Chapter 2

Theory

2.1 Thermoresponsive behaviour of pNipam

As can be seen in figure 2.1, the monomer of which pNipam is made up, is an amphiphilic molecule. The isopropyl moiety acounts for the hydrophobic interactions, while the amide moiety is relatively hydrophilic. The equilibrium between the hydrophobic and hydrophilic interactions of this molecule in water is governed by the temperature. At low temperature (T < LCST), the hydrophilic character dominates, meaning that the volume of crosslinked microgel particles consists mainly of water. At elevated temperature (T > LCST) the hydrophobic interactions start to dominate, expelling the water from the particles' interior, hence losing up to 90% of its volume. This responsive behaviour can, in principle, also be triggered by stimuli other than varying temperature. Especially with incorporation of comonomers, it is possible to alter the radius as a function of other external stimuli. For example, copolymerization with AAc introduces a pH-response to the LCST.[15,16,20]

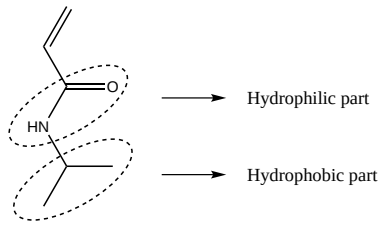

Figure 2.1: Chemical structure of the monomer of pNipam in which its hydrophilic and hydrophobic region are indicated.

2.2 Phase behaviour of colloids

The phase behaviour of colloids was first predicted in 1957 by Alder *et al.*[21] They reported of the seperation in a concentrated and diluted phase in concentrated systems of hard spheres based on computer experiments. In 1986, Pusey *et al.* were the first to confirm this phase behaviour.[8] They used particles which were fairly monodisperse (polydispersity of 5 %), and with a steep repulsive potential. With this system they tried to mimic the theoretical hard sphere system and showed their behaviour when their volume fraction is increased. Figure 2.2 shows their findings.[22] After a equilibration time, the more concentrated samples tend to form crystals, or glasses when the concentration is even higher. This result is analog to the behaviour of atoms/molecules upon increase in density.

2.3 Emulsion polymerization

Since rubber has become an important resource in the industry, a lot of research has been conducted towards polymer synthesis. This led to the understanding of the method called emulsion polymerization. By now the use of this method is not only limited to rubber, but has also found his way towards colloid science. For example, the method is used for preparation of polysterene, polymethylmethacrylate and also pNipam particles.[23,24]

Figure 2.2: The phase behaviour of colloidal crystals, as function of their volume fraction. In relatively concentrated sample, crystal and glass formation is observed.

The name of this method arises from the fact that the starting point of the reaction is an emulsion. The solvent is the continuous phase, with the liquid monomer as the dispersed phase. To prevent seperation of both immiscible liquids, vigorous stirring or addition of a surfactant is necessary. In the case of this thesis, all the syntheses were performed surfactant-free. The polymer should also be immiscible with the solvent. Otherwise, dissolved polymer will be formed, which will not form well-defined sphere-like particles.

The course of emulsion polymerization is governed by three important steps. The first one is the initiation by a water-soluble radical initiator. In the case of pNipam preparations, KPS or APS are mostly used. Upon heating the mixture, the weak oxygen-oxygen bond will dissociate, leaving both fragments with an unpaired electron, making the fragment a radical (figure 2.3). This radical is able of attacking the monomer molecule, hereby transferring the unpaired electron to the monomer. The monomer itself can now attack other monomers in the second step, called propagation (figure 2.4). The final step in all radical-initiated polymer synthesis is that of termination. In this step, two growing chains meet, combining their unpaired electrons in an electron pair, losing the ability to propagate.

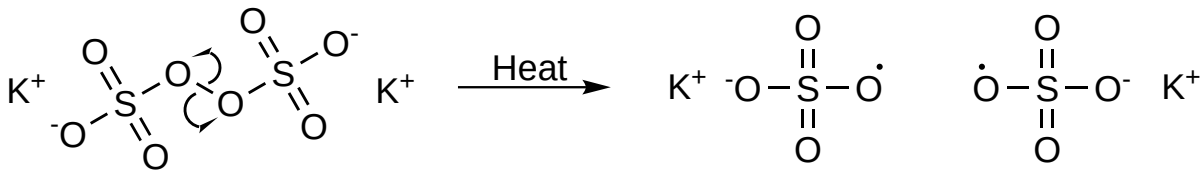

Figure 2.3: Reaction scheme of the thermal dissocation of KPS. In this process two radical fragments are formed due to the heating of KPS, a generally used water-soluble radical initiator.

A complete overview of the formation of pNipam microgels in a surfactant free reaction mixture, is shown in figure 2.5. During the reaction, a small amount of monomer is in solution, due to equilibrium (**A**). The initiator will initiate the reaction by attacking a free monomer and propagation will occur (**B**). After a short time of propagation, the polymer chains reach a certain length at which they are not soluble anymore. At this stage, the polymer chain is stabilized by the charge on its surface, which originates from the initiator. The chain can now be considered a seed particle (**C**). Due to incorporation in polymer, free monomers leave the emulsion. Because of equilibrium, more monomer can dissolve and will react, ending up in the polymer. In this way the monomer droplets are slowly consumed and allow the seed particles to continue to grow to form particles (**D**). Because of the slow but steady consumption of monomer, this synthesis method is capable of producing large, monodisperse particles.

During the synthesis, the crosslinker also plays an important role. In principle, this comonomer is incorporated in the same way during the propagation, although minor differences might be possible. For

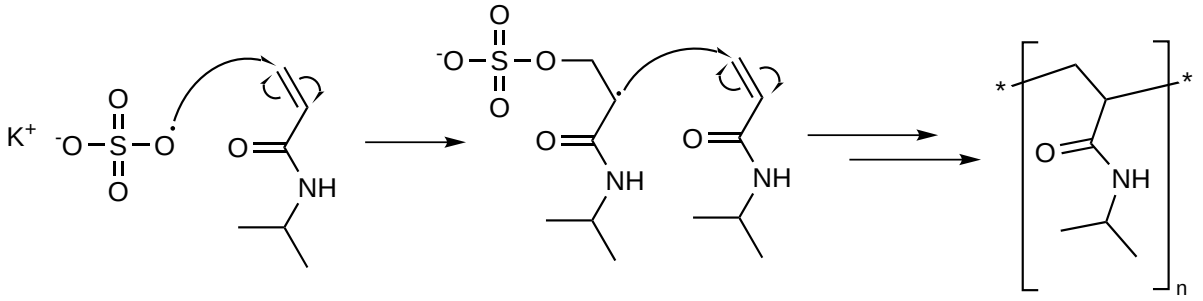

Figure 2.4: A reaction scheme of KPS attacking Nipam in the first step (initiation). In the second step the reaction propagates, when the radical on the Nipam molecule attacks another Nipam molecule. Upon continuation of this proces, a polymer chain will be formed (last step). The process of propagation in the case of KPS as initiator and Nipam as monomer.

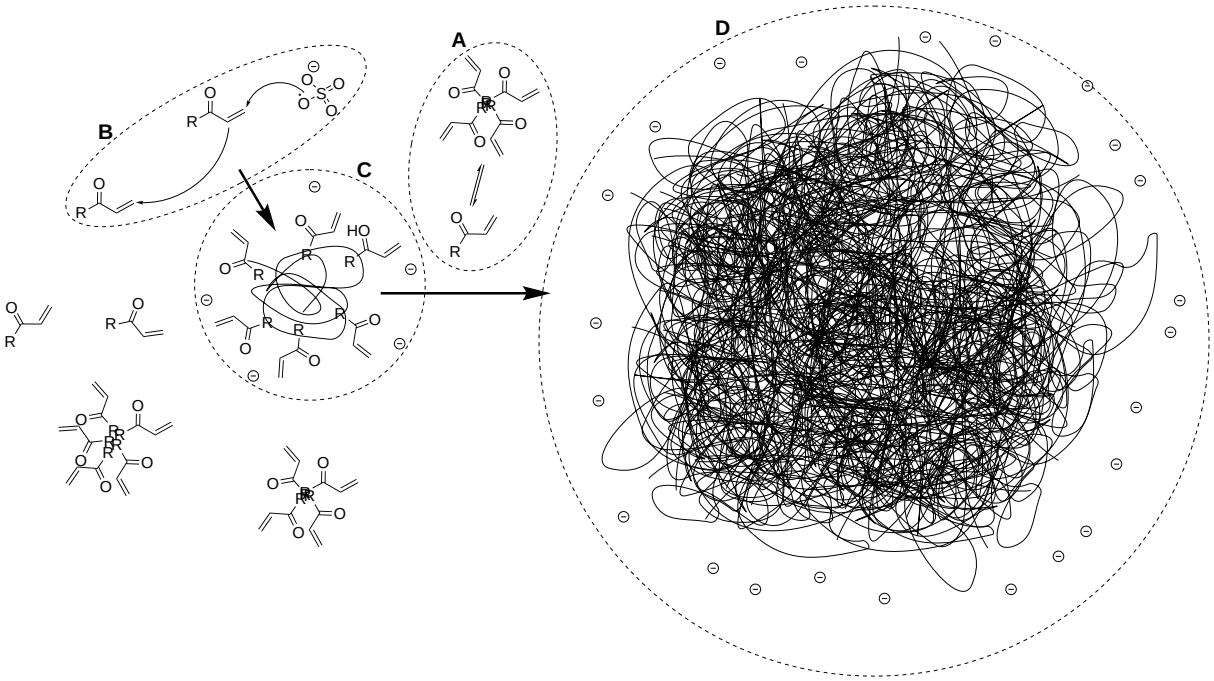

Figure 2.5: A schematic overview of emulsion polymerization based pNipam synthesis. **A** depicts a monomer micelle, which will gradually be consumed. **B** shows the process of initiation and propagation with dissolved monomers. **C** depicts a particle seed, which has become insoluble and is stabilized by its surface charge. Finally, **D** depicts a pNipam particle.

instance, for BIS, the crosslinker used in all preparations in this thesis, it is known that polymerization rate is higher than that of Nipam.[25] This will lead to less homogeneous particles, which have more crosslinker in the core than in the shell. There are ways to produce more homogeneous particles, by applying crosslinking monomer feed during the reaction.[26] The heterogenenity of crosslinking influences the particles behaviour. The core-shell particles will have relatively long polymer changes protruding from the core. These polymer chains will account for steric stabilization. When the particles are crosslinked throughout the whole particles, the protruding chains will be shorter. Other effects include changes in the hydrodynamic radius, as the flow of water through the outer shell will be different in both cases.

2.4 Light scattering

In colloid chemistry, two major characterization techniques are based on light scattering: static light scattering (SLS) and dynamic light scattering (DLS). To understand these techniques, one first has to understand the underlying principle of interaction between light and simple objects. When a very small particle ($r \ll \lambda$) is illuminated, this particle will scatter light according to the Rayleigh approximation:

$$I_{scattered} = I_0 \frac{1+\cos^2\theta}{2R^2} \left(\frac{2\pi}{\lambda}\right)^4 \left(\frac{n^2-1}{n^2+2}\right)^2 \left(\frac{d}{2}\right)^6 \tag{2.1}$$

It can be seen from this equation, that the scattered intensity is a function of the angle θ. When one illuminates a larger particle ($r \geq \lambda$), the particle scatters the light as if it is a collection of point scatterers. The light originating from the many points in the particle, will interfere with each other. This scattered signal is of a very high complexity. Only a few systems can be solved analytically (like spheres, by using Mie theory). However, upon doing deriviation, which will be omitted for convenience, one comes to the following proportionality:

$$I(q) \propto P(q) \tag{2.2}$$

Here, $P(q)$ is called the form factor and q is the wave vector, given by:

$$q = |q| = \frac{4\pi n_0}{\lambda} \sin\left(\frac{\theta}{2}\right) \tag{2.3}$$

The interference from the collection of point scatterers is dependent on the distribution of them, i.e. on the size and shape of the particle. Therefore, the form factor contains size- and shape related information. For a sphere, the form factor is known and described by:

$$P(q) = \left[3 \cdot \frac{\sin(qa) - qa\cos(qa)}{(qa)^3}\right]^2 \tag{2.4}$$

with a being the sphere's radius.

Upon considering several particles relatively close to each other, another contribution plays a role in scattering. In this case, light scattered by the invidual particles will also meet and interfere, complicating the scattered signal even more. The proporionality with the form factor still applies, and another variable enters the proportionality:

$$I(q) \propto P(q) \cdot S(q) \tag{2.5}$$

Since the structure factor arises from interference of scattered light of particles close to each other it contains information which can lead to the pair distribution function. In the very diluted regime, this interference is absent, so the structure factor is one. In this way, the form factor can be obtained, hence our measurements were all carried out in the diluted regime.

2.4.1 Static light scattering

An SLS measurement consists of measuring the intensity of scattered light through a sample at various angles (figure 2.6). To achieve this, the colloidal system is illuminated in a cylindrical cuvet. The sample will scatter the incident beam in all directions. The scattering intensity will be measured by a light detector at various angles. The obtained angular dependency is related to size and polydispersity of the system. When one plots the logarithm of the intensity against the wave factor squared, one obtains the form factor. Figure 2.7 shows the overlay of such a SLS measurement on the form factor of a sphere (as described by equation 2.4). With a as the only variable in a sphere's form factor, the SLS plot can be used to derive the radius. Since pNipam is not a homogeneous sphere, fitting is more complex in that case. Stieger *et al.* developed a fitting model for pNipam particles based on small angle neutron scattering, which was successfully applied by Meyer *et al.* on SLS results.[27,28]

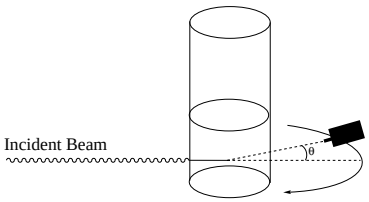

Figure 2.6: A schematic overview of a SLS setup. The light from the incident beam scatters in the sample. The angular dependancy of the scattered intensity is measured with a mobile detector.

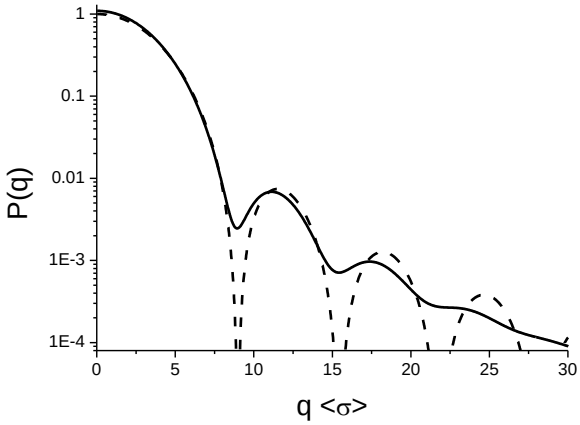

Figure 2.7: A plot of a SLS measurement (solid line), superimposed on a sphericals particle theoretical form factor (dashed line). Picture courtesy of Andrei Petukhov.

Guinier range

As was shown in previous subsection, the form factor can be used to derive size and shape information. However, this method is relatively complex. A more straightforward way to obtain size information is a Guinier analysis. As can be seen from equation 2.6, when the $ln(I)$ is plotted against q^2, the slope of the tangent at low q-values can be used to derive the radius of gyration.

$$P(q) = 1 - \frac{1}{3}q^2 R_g^2 + \dots \tag{2.6}$$

For a sphere the relation between the actual radius R and the radius of gyration, R_g, is given by the relation in equation 2.7.

$$R_g = \sqrt{\frac{3}{5}R} \tag{2.7}$$

2.4.2 Dynamic light scattering

In DLS measurements the time-dependent fluctuation of the scattered intensity is measured at a fixed angle (figure 2.8). Due do Brownian motion the particles perform random movement, which will cause the scattered signal to change. When a very small area is observed with a detector, the altering scattered intensity can be measured. When plotting the result, the fluctuation of signal in time is obtained. Because of the high time-resolution of the detector, and the finite velocity of the particles, there is a correlation in the alternation of the light. This correlation depends upon the speed with which the particles move. Faster moving particles will cause the signal to fluctuate faster than larger particles will. Since the speed of the particles is dependent upon their size (and temperature and viscosity), the correlation in the signal can be used to derive size-information of the particles in the system measured with DLS (figure 2.9).

The correlation in the signal is calculated using equation 2.8 and it can be easily seen that at very short time scales (τ is small), the correlation is close to one. This is due to little movement of the particles on this short time scale.

$$g^2(q;\tau) = \frac{< I(t)I(t+\tau) >}{< I(t) >^2} \tag{2.8}$$

In the case of a monodisperse system, the correlation function is a single exponential decay as described by

$$g^1(q;\tau) = \exp(-\Gamma\tau) \tag{2.9}$$

In this case Γ is the decay rate, and it is related to the translational diffusion coefficient D_t according to

$$\Gamma = q^2 D_t \tag{2.10}$$

The Stokes-Einstein relation relates the diffusion coefficient to the hydrodynamic radius (R_H) of a sphere:

$$D_t = \frac{k_B T}{6\pi\eta R_H} \tag{2.11}$$

After obtaining the R_H it is important to realize that this parameter is related to a spherical particle. It means that the observed particles behave in the same way as a sphere with radius R_H would do. The R_H is influenced by the layer of water dragged around by the particles. Particles with a loosely crosslinked shell (like the pNipam systems), have an outer region through which water can readily move. For this reason the hydrodynamic diameter of pNipam is smaller than its actual diameter. When the term "diameter" is used discussing DLS results, this refers to $2 \cdot R_H$.

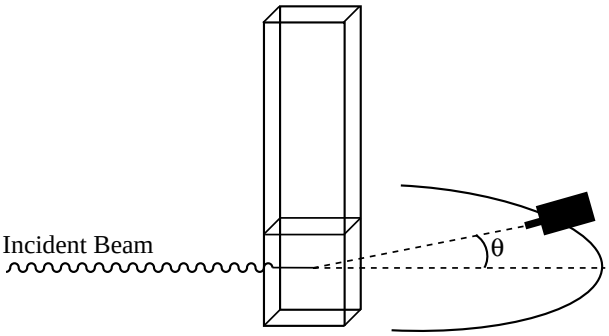

Figure 2.8: A schematic overview of a DLS setup. The incident beam enters the sample and gets scattered by the particles. A detector with a very small detection area, measures the intensity of the scattered light at a fixed angle.

2.5 Electron microscopy and pNipam microgels

Since light microscopy can only be used to observe relatively large particles ($d \geq \lambda_{visible\,light}$) other waves can be used. Electron microscopy techniques make use of the fact that the de Broglie wavelength of an highly accelerated electron is much smaller than that of visible light, as shown in:

$$\lambda = \frac{h}{p} \tag{2.12}$$

Thus, electrons can be used to visualize particles which are at the limit of optical visibility. Furthermore, in pNipam systems, the difference of refractive index with the solvent is very low, complicating visible light microscopy even more. Since electron microscopy is not carried out with a dispersed sample, that problem is also solved.

Despite the advantage of electron microscopy, there are also some drawbacks. For electron microscopy, an ultrahigh vacuum is necessary, thus the sample needs to be dried. In case of solid particules (like metallic ones), drying does not have a rigorous effect. In case of pNipam particles however, there is such an effect, because PNipam particles consist mainly of water, which will be removed upon drying. Therefore, the structure of the particles changes to a collapsed state, as can be made visible by using SEM (figure 2.10).[16] Due to this effect, information of the exact size of the original particles gets lost.

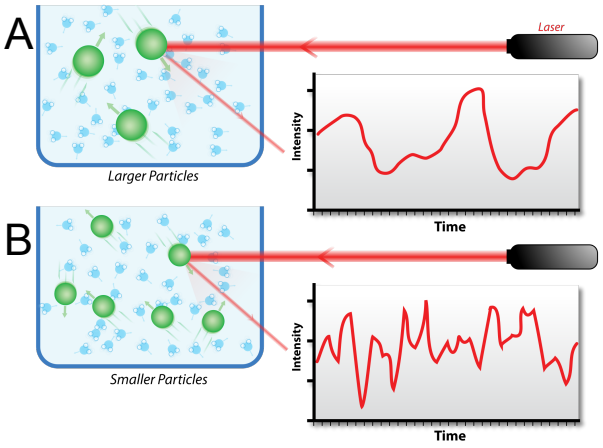

Figure 2.9: A schematic overview of the origin of a DLS result. A) The particles are relatively large. Therefore, they move relatively slow, leading to slow fluctuations in the scattered intensity. The intensity-time plot is quite smooth in such a case. B) Smaller particles are measured. They move relatively fast, making the signal fluctuate a more on shorter time scales. For this reason the intensity-time plot has sharper peaks and is less smooth. Picture is original work from wikipedia.org.

Also, the information about shape and structure is not reliable anymore. For this reason, TEM can only be used to confirm the presence of particles and to speculate about order of magnitudes and structural properties.

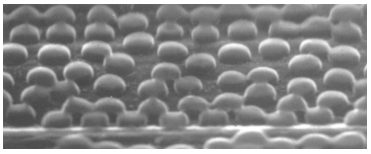

Figure 2.10: SEM micrograph of pNipam particles, revealing the collapsed structure after drying.

Apart from the collapse of individual particles, interpenetration of the polymer networks might also be observed, an example is shown in figure 2.11. A last illustration of the effect of drying is shown in figure 2.12. On these TEM micrographs three regions, introduced by drying, can be distinguished. The first region (upper right corner), shows small aggregates of particles. The second region consists of distinct single particles, whereas the third region seems to be made up of a network of interpenetrated particles. Furthermore, the chosen way of electron microscopy sample preparation and drying might influence the system, leading to several other effects. Whereas drying is performed under a heating lamp most of the time during this research, it is also possible to dry the samples in ambient conditions. In this way, the effects might be less vigorous. However, even if the drying effects are minimalized, the measurement itself will still influence the sample. During electron beam illumination, a lot of energy is transferred towards the sample, altering the particles appearance.

For the above reasons, one has to be very cautious upon interpreting TEM studies of microgels. TEM can be a useful tool in determining wether particles are present and what their typical sizes are. However, one can never literally translate the results of TEM to the particles in the original suspension.

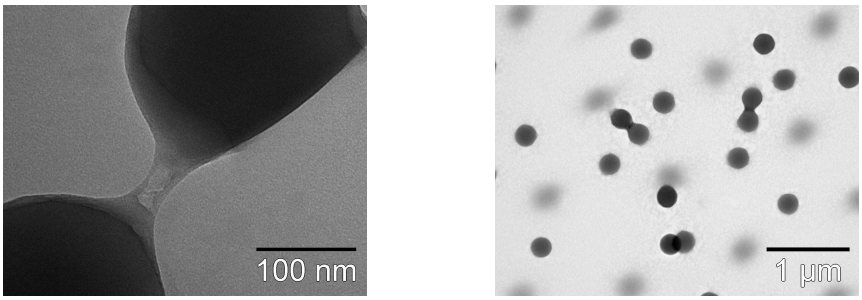

Figure 2.11: TEM micrographs showing the drying induced interpenetration of pNipam polymer networks.

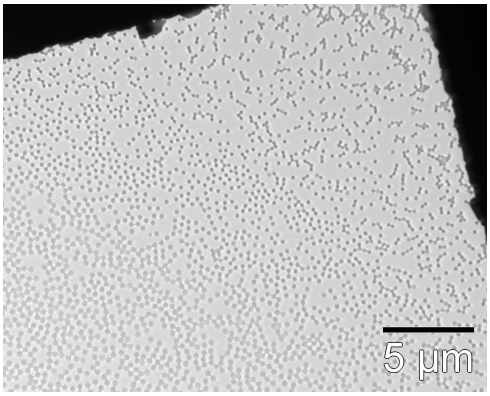

Figure 2.12: TEM micrograph revealing three regions of pNipam particles, due to drying effects.

2.6 Confocal microscopy

Confocal microscopy is an optical technique which can be used to image fluorescent samples. A schematical presentation of a setup is shown in figure 2.13. The sample will be illuminated with laser light. If the laser has a wavelength low enough ($\lambda \leq \lambda_{excitation}$), excitation will occur. After being excited, the material will emit light with a higher wavelength ($\lambda = \lambda_{emission}$). This light will be seperated from the incident beam by a beam splitter. The signal is then projected on a detector, after passing a small aperture. Due to the point illumination and the removal of out-of-focus light by the aperture, a very high resolution in a single sample plane can be obtained. After scanning several planes of the sample it is possible to make a 3D reconstruction. The properties of confocal microscopy make it a very useful technique, provided that the particles are large enough. When one wants to make 3D reconstructions, particles' diameter should be around or above 1.0 µm.

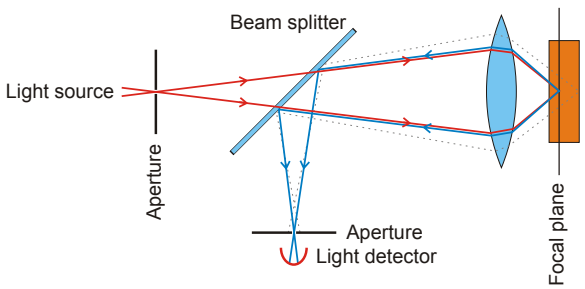

Figure 2.13: A schematical representation of a confocal microscopy setup. The path of the incident beam and the fluorescent signal (solid lines) are shown, as well as the out-of-focus signal (dashed line).

Chapter 3

Experimental section

3.1 Materials

In this subsection, the supplier and purity of the used chemicals are listed. AAc (Sigma Aldrich, 99 %), APS (Acros, 98 %), BIS (Sigma Aldrich, 98 %), 1-butanol (Acros, 99 %), diethylether (Sigma Aldrich, 0 %), ethanol (Interchema, pure), KPS (Acros, 99 %), MAE (Acros, 99 %), PolyFluor 570 (Polysciences Inc., purity not denoted), methacryloylchloride (Fluka, 97 %), methanol (Baker, 99.5 %), NBD-Cl (Acros, 98 %), pNipam (Sigma Aldrich, 97 %) and 1-propanol (Acros, 99 %) were used as received, without any further purification.

TEA (Sigma Aldrich, 99.5 %) and toluene (Interchema, practical grade) were distilled and dried over 3 Å molecular sieves (Fluka) prior to use in the NBD-MAEM synthesis.

3.2 Synthesis of NBD-MAEM

One of the fluorescent dyes, NBD-MAEM, was synthesized as described in this section. The reaction scheme is depicted in figure 3.1. [29]

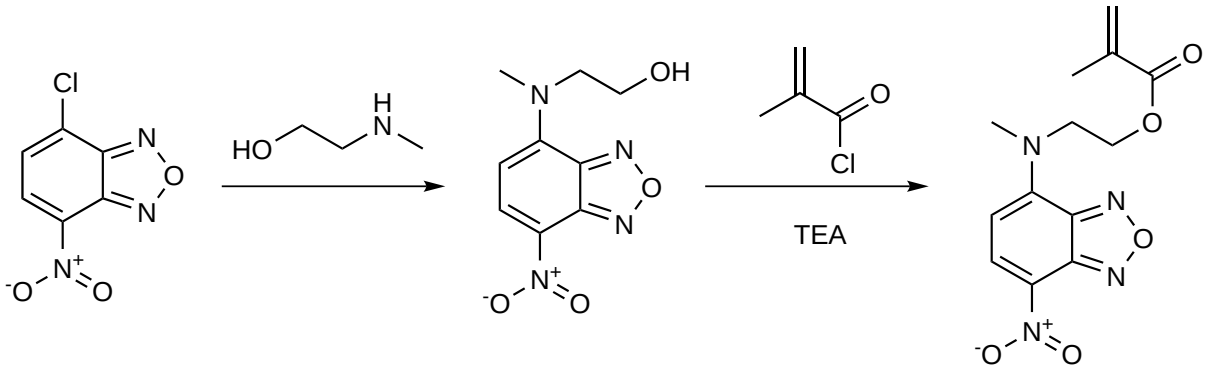

Figure 3.1: Reaction scheme of the preparation of NBD-MAEM with NBD-Cl as starting material. First step: NBD-Cl is reacted with 2-(methylamino)ethanol to form NBD-MAE. Second step: NBD-MAE reacts with methacryloyl chloride to form NBD-MAEM.

First, NBD-Cl (2.763 g, 13.7 mmol) was dissolved in a Schlenk flask in ethanol (180 mL). MAE (6.62 g, 88.1 mmol) was dissolved in ethanol (32 mL) in another Schlenk flask. Both Schlenk flasks were evacuated and flushed with nitrogen three times. The solution of MAE was transferred to the Schlenk flask with the NBD-Cl-solution, together with an additional amount of ethanol (20 mL). The mixture was stirred under nitrogen atmosphere for 90 minutes and turned from yellow to dark orange under formation of precipitate. Afterwards, the mixture was filtered using a Büchner funnel and reduced pressure. The residue was washed with a cold (−20 °C) 70/30 (v/v) methanol/diethylether mixture and was dissolved in ethanol (1 L) of 60 °C, before storing it at −20 °C. Subsequently, the mixture with NBD-MAE crystals was filtered with a Büchner funnel and the crystals were washed with cold ethanol (−20 °C). Next, the NBD-MAE was dried in a Schlenk flask by flushing it with nitrogen for 2 days before evacuating it while heating to 45 °C. NBD-MAE was obtained as a dry orange flakes.

The conversion of NBD-MAE to NBD-MAEM was carried out entirely in a glovebox under nitrogen atmosphere. First, NBD-MAE (0.367 g, 1.54 mmol) and TEA (32 mL) were added to dry toluene (50 mL). Althought the NBD-MAE did not totally dissolve, methacryloylchloride (0.2 mL, 2.0 mmol) was added under stirring. The appearance of the precipitate changed, indicating formation of an ammonium salt. After 2 hours of stirring, the mixture was filtrated and the filtrate was evaporated and dried under reduced pressure. The obtained material was a red oily material, which was purified by means of column chromatography over silica gel. For elution a gradient was used, starting with an 2/1 (v/v) acetate-n-hexane mixture, ending with a 1/1 (v/v) mixture. To confirm purity, ^{1}H and ^{13}C NMR spectroscopy were performed.

3.3 Synthesis of pNipam microgels

3.3.1 General protocol

All pNipam systems were prepared by surfactant-free emulsion polymerization in an aqueous solution of Nipam and BIS, with addition of a radical initiator (KPS or APS). All preparations were performed in milliQ water under a nitrogen atmosphere. To prevent nucleation on the glass surface, overnight cleaning with etching fluid (KOH, ethanol and water) can be performed, prior to reaction. In a typical synthesis, milliQ water (100 mL) was degassed in a 250 mL round-bottom flask by applying a nitrogen flow while stirring vigorously. The nitrogen flow was maintained for at least 1 hour prior to initiation, to be sure all oxygen was removed. Nipam and BIS were added during the nitrogen purging process and the mixture was heated using an oil bath (to 70 °C, unless stated otherwise). Heating was performed under reflux cooling, stirring and appliance of a gentle nitrogen flow, to prevent inflow of oxygen. The setup described is shown in figure 3.2, and was left unadapted during the reaction.

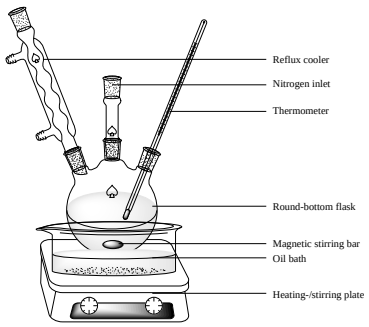

Figure 3.2: The experimental setup used for pNipam syntheses.

During the purging/heating process, an amount of radical initiator (KPS or APS) is dissolved in a small amount of water (ranging from 3 to 5 mL). When the temperature was stable at the desired temperature, the radical initiator solution was added to the mixture. If any other additional reactants were needed, they were added either before radical initiator addition, or during the course of the reaction. The additional reactants consist of dye (in a specific solvent) and/or AAc. After initiation, heating was maintained for at least 1 hour, assuming that most monomer reacted in this time. Afterwards, the mixture was allowed to cool while maintaining stirring, or by tumbling in a centrifuge tube. To remove excess monomer, the successful batches were washed by means of centrifugation for a maximum of 2 to 3 days, depending on particle size, at 2500 rpm. Then, the supernatant was decantated or removed by a pipette and the particles were redispersed in milliQ water up to the original volume (normally 100 mL). A system was considered monomer-free after three consecutive centrifugation procedures.

3.3.2 Synthesis of pNipam microgels

Several preparations of regular pNipam were performed, both to become familiar with the synthesis as well as to test several parameters, like solvent dependency. The synthesis was performed according to the protocol described in section 3.3.1. The amounts of materials used are listed in table 3.1.

3.3.3 Synthesis of pNipam-co-AAc microgels

PNipam-co-AAc preparations were performed to check whether this would produce bigger particles. The synthesis was carried out by adding an amount of AAc (95 µL), before adding the initiator solution. The preceding and succeeding steps are as in the regular pNipam synthesis (3.3.1). The amouns of materials used in these preparations can also be found in table 3.1.

3.3.4 Synthesis of pNipam microgels with incorporation of NBD-MAEM

To prepare NBD-MAEM incorporated pNipam microgels, the normal protocol (section 3.3.1) was adapted by adding a small amount of NBD-MAEM-solution (in a given solvent) before addition of initiator solution. In several cases, a small amount of NBD-MAEM-solution was also added after initiation. The typical amounts of dye added were around 1 to 20 mg, and the solvents used were 1-butanol, ethanol, propanol, toluene or the reaction mixture itself (which is milliQ water based). The used amounts of materials are listed in table 3.2.

Since the synthesis of dyed pNipam was complexer than expected, stabilizing factors were necessary. In the following three subsections, stabilization is attempted by means of: higher crosslinker/initiator concentrations; AAc incorporation and buffer stabilization. This was done both with NBD-MAEM and PolyFluor 570 as dye.

3.3.5 Synthesis of pNipam with dye incorporated in high crosslinker/initiator concentrations

The high concentration crosslinker/initiator preparations involved altering the protocol (3.3.4) by using the amounts listed in table 3.2. This synthesis protocol was also done once without addition of dye, to test the protocol.

3.3.6 Synthesis of pNipam-co-AAc microgels with dye incorporated

PNipam-co-AAc microgels were synthesized based upon section 3.3.4, except for the addition of AAc (95 µL, 1.4 mmol), which was added just before initiator addition. The syntheses were performed with NBD-MAEM or with PolyFluor 570, with the amounts listed in 3.2.

3.3.7 Synthesis in acetate buffer

In this synthesis, pNipam microgels were prepared in an acetate buffer. Acetate buffer was prepared by mixing acetic acid (2.720 g, 45.3 mmol), sodium hydroxide solution (9.0 mL, with a concentration of $1\,\mathrm{mol}\cdot\mathrm{L}^{-1}$) and milliQ water, up to a total of 1.0 L. The preparation of the particles was again based on section 3.3.4, with the milliQ water being replaced with the acetate buffer. Amounts of reactants used are listed in table 3.2.

3.3.8 Other parameters

Next to variation in the used materials and their relative amounts, there are a lot of other parameters which can be altered. Amongst these possible variations are temperature, stirring speed, amount of used water and amount of used organic solvent to dissolve the dye. It would be inconvenient to mention all individual changes which have been made to the reaction protocol for all the synthesized batches. For convenience, the changes will only be mentioned when relevant.

3.4 Analysis of pNipam systems

3.4.1 TEM

TEM measurements were performed using a Philips Tecnai 10 and Tecnai 12. It was used to determine the presence of particles. TEM could also be used to estimate roughly the dimensions of the particles, as well as its internal structure. However, it always has to be kept in mind that drying effects might alter the size and structure of particles. To prepare a sample for a TEM measurement, a 100 times diluted dispersion was prepared by adding 100 µL of concentrated sample to 10 mL of milliQ water. Afterwards,

a drop of the diluted dispersion is applied with a pasteur pipette on a TEM grid. The sample was then concentrated by evaporation under a heating lamp.

3.4.2 DLS

The DLS measurements were carried out on a Malvern Zetasizer Nano at two fixed angles: 173° for backward scattering measurements, and 12.8° for forward scattering experiments. To prepare a DLS sample, a diluted sample was prepared by diluting the mixture (at reaction concentration) (typically 100 to 200 times). Prior to measurement, the diluted sample was filtrated through a 5 µm filter to remove dust. Disposable cuvets were used to perform the DLS measurement.

3.4.3 SLS

The SLS measurements were carried out on a custom built setup. For illumination a Hg-lamp was used. Filters were used to make the light monochromatic with a wavelength of 546.1 or 578 nm. The measurements were performed from 20° to 120°, with steps of exactly 1°. The samples were diluted and filtrated in exactly the same way as for DLS (section 3.4.2). A cylindrical shaped cuvet was used and immersed in a temperature controlled toluene bath during the measurement.

3.4.4 Confocal microscopy

A Nikon Eclipse TE2000U inverted microscope with a Nikon C1 confocal scanning head was used to obtain images. The lasers used for illumination were a Spectra Physics 163C air cooled ion laser operated at a wavelength of 488 nm for NBD-MAEM-dyed particles and a Melles Griot laser operated at 543.5 nm for particles dyed with PolyFluor 570. To do a confocal microscopy measurement, measurement cups are prepared using Chromacol 2-SV vials and Menzel Gläser 22 mm #1 microscope cover slips. The bottom of the vials was removed and cover slips were glued to the bottom of the vials using Bison Kombi Snel two component epoxy glue. Since the measurements were performed in water, solubility of the glue in organic solvents was not an issue. A small amount (0.1 to 1 mL) of concentrated sample was placed inside the cup for measurement.

Table 3.1: A list of the preparations of pNipam without fluorescent dye. Both normal crosslinked pNipam syntheses, as well as crosslinked pNipam-co-AAc preparations have been performed.

#	Nipam (g)	BIS (mg)	KPS (mg)	APS (mg)	Added solvent
Regular pNipam preparations					
DLM1.1	1.3	26	52		
DLM1.2	1.3	26	52		
DLM1.3	1.3	26	52		
DLM1.4	1.3	26	52		
DLM1.5	1.3	26	52		
DLM4.1	1.3	40	40		
DLM31	1.35	28	54		toluene
DLM33	1.4	40	40		
DLM34	1.4	40	40		
PNipam-co-AAc preparations					
DLM15	1.4	32		50	
DLM15.2	1.4	32		50	
DLM35	1.4	40	40		
DLM36	1.4	40	40		
DLM37	1.4	40	40		toluene
DLM38	1.4	40	40		ethanol
DLM39	1.4	40	40		butanol

Table 3.2: A list of all the performed pNipam-co-dye syntheses. The preparations are categorized in one of four categories: a variation of the regular pNipam synthesis; synthesis in acetate buffer; synthesis with increased amounts of crosslinker and initiator; synthesis of dyed pNipam-co-AAc.

#	Nipam (g)	BIS (mg)	KPS (mg)	APS (mg)	Dye	Dye amount (mg)	Dye solvent
PNipam-co-NBD-MAEM preparations							
DLM3.1	1.3	26	52		NBD	4	ethanol
DLM3.2	1.3	26	52		NBD	4	ethanol and water
DLM3.3	1.3	26	52		NBD	4	ethanol and water
DLM5.1	1.3	26	52		NBD	26.5	ethanol and water
DLM6.1	1.3	26	52		NBD	27.5	propanol
DLM7.1	1.3	40	40		NBD	13.75	propanol
DLM8.1	1.3	26	52		NBD	11	toluene
DLM9.1	1.3	40	40		NBD	13.2	toluene
DLM9.2	1.3	40	40		NBD	10	toluene
DLM13	1.3	27	54		NBD	0.7	ethanol
DLM14	1.3	26	54		NBD	2	ethanol
PNipam-co-dye preparations in acetate buffer							
DLM11	2	46		53	NBD	4.6	propanol
DLM12	2	46		56	NBD	4.6	propanol
DLM18	2	48		52	NBD	4	isobutanol
DLM19	1.44	37		51	NBD	4	isobutanol
DLM32	2	50		56	Rho	1	ethanol
PNipam-co-dye preparations with high concentration crosslinker and initiator							
DLM17	1.9	136	100		NBD	2	reaction mixture
DLM20	2	136	100		Rho	2	reaction mixture
DLM21	2	136	70		Rho	1	reaction mixture
DLM22	2	136	100		Rho	1	reaction mixture
DLM23	2	134	74		Rho	0.9	ethanol
DLM24	2	132	73		Rho	0.9	ethanol
DLM25	2	131	101				
DLM26	2	136	103		Rho	2.3	ethanol
PNipam-co-AAc-co-dye preparations							
DLM10	1.4	31		51	NBD	9.2	toluene
DLM16	1.4	34		52	NBD	2	reaction mixture
DLM27	1.4	40	40		Rho	1.74	ethanol
DLM27.2	1.4	40	40		Rho	1	ethanol
DLM28	1.4	40	40		Rho	1	ethanol
DLM29	1.4	40	40		Rho	1.1	ethanol
DLM30	1.4	40	40		Rho	1.6	ethanol
DLM40	1.4	40	40		Rho	2.3	1-butanol
DLM41	1.4	40	40		NBD	4	toluene

Chapter 4

Results and discussion

4.1 Non-fluorescent pNipam microgel synthesis

To become familiar with pNipam synthesis and to check if the protocols work as expected, preparations without dye have been performed. This has been the case for both normal pNipam as well as pNipam-co-AAc microgel preparations.

4.1.1 Regular pNipam microgel synthesis

Regular pNipam was synthesized several times according to section 3.3.2. At first sight, none of these reactions showed unexpected behaviour. During the reactions, turbidity increased 5 minutes after initiator addition and kept increasing untill the dispersion was totally opaque. Upon cooling, the opacity decreased slightly due to a change in the particles' refractive index. The cooling induces swelling, which introduces more solvent in the interior of the particle. In this way, the refractive index difference between the surrounding solvent and the particles becomes smaller. The extent of swelling is related to the amount of crosslinking in the particles. For this reason, the change in turbidity gives information about the crosslinker content in the particles.

The pNipam systems were characterized by means of SLS. The SLS curves at room temperature ($T = 20.5\,^{\circ}\mathrm{C}$) for DLM1.1, DLM1.2, DLM1.3 and DLM1.4 are shown in figure 4.1-a. From the figure, it can be seen that the curves are comparable. This indicates that the result of the synthesis is reproducable. For DLM1.2, its temperature behaviour has been briefly explored. SLS curves of this sample were recorded at both 20.5 and 35.0 °C (figure 4.1-b). The change in curves upon heating reveals the thermoresponsive behaviour of the system because a shift in minima towards higher q-values indicates smaller particles.

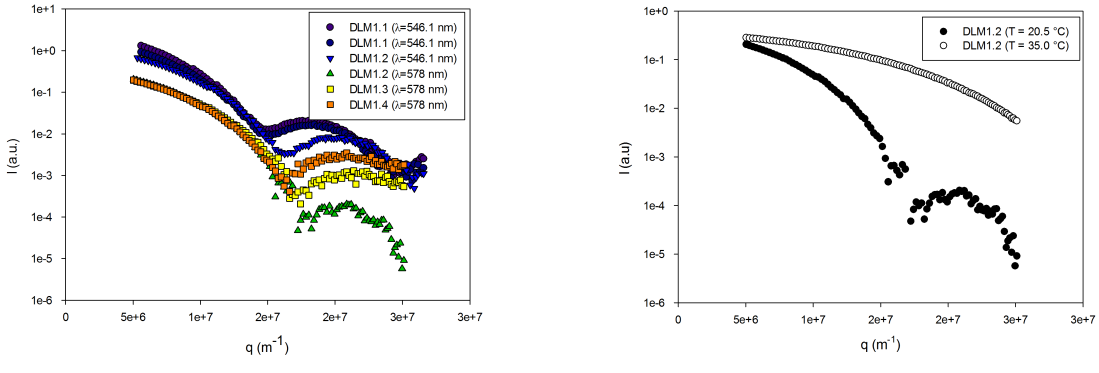

(a) **(b)**

Figure 4.1: **(a)** SLS curves recorded from diluted samples of systems DLM1.1, DLM1.2, DLM1.3 and DLM1.4, which are all regular pNipam microgel systems. The temperature during the measurements was 20.5 °C. **(b)** SLS curves recorded from a diluted sample of DLM1.2 as function of temperature. The wavelength used for these measurements was 578 nm.

By using the Guinier approximation, the radius of gyration of the particles can be obtained. The radii of gyration are used to calculate the diameter of a corresponding homogeneous sphere. The calculated

radii are displayed in table 4.1. From this table it can be concluded that the particles are in the same order of magnitude, so it is possible to reproducibly prepare pNipam microgels. The numbers can however not be used to be conclusive about their dimensions. PNipam is known to be core-shell like. For this reason, more complex fitting methods are necessary to obtain the exact size.

Table 4.1: The calculated radii of gyration and approximated diameter of DLM1.1, DLM1.2, DLM1.3 and DLM1.4. These numbers were calculated by using the Guinier approximation and assuming homogeneous spherical particles.

Batch number	Temperature (°C)	R_g (nm)	Approximated diameter (nm)
DLM1.1 (first measurement)	20.5	265	684
DLM1.1 (second measurement)	20.5	260	671
DLM1.2 (first measurement)	20.5	242	625
DLM1.2 (second measurement)	20.5	241	622
DLM1.3	20.5	233	602
DLM1.4	20.5	240	620
DLM1.2	35.0	127	328

Several DLS measurements were done with system DLM1.2, to obtain complementary information. The plot of the average diameter as function of temperature (at 25, 35 and 50 °C) is shown in figure 4.2. There is a clear difference between the forward and backward scattering results, with the former always giving lower values for the R_H. However, since forward scattering penetrates into the sample more, the signal strenght is also stronger, which leads to a more consistent result in forward scattering too. Other regular pNipam systems have not been characterized with DLS, but comparable results are expected, based upon the similarity in SLS measurements.

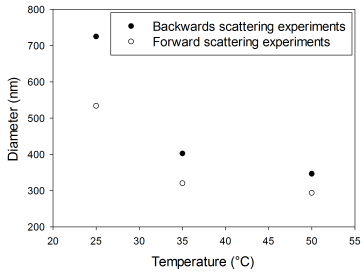

Figure 4.2: The average of the diameter of system DLM1.2, based upon 5 measurements.

TEM has been used to obtain information about the particle appearance. Especially notable are the TEM micrographs of DLM1.2, which reveal 2D ordering (figure 4.3). It is unclear at what point during the heating/drying process this ordering originates from. For this reason, it is impossible to be conclusive using the interparticles distance of these micrographs. The fact that particles are observed on "interstitial" positions indicates that there was a second (incomplete) layer with ordering.

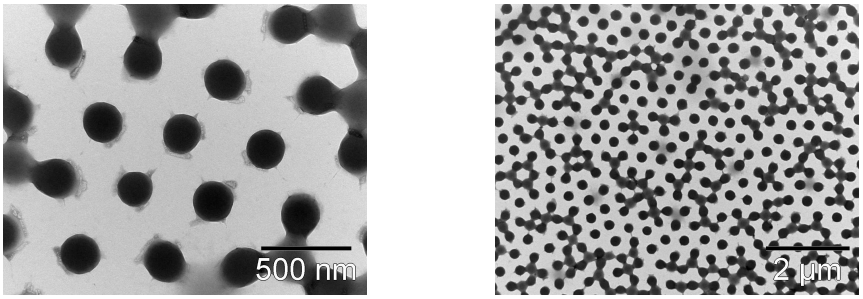

Figure 4.3: TEM micrographs revealing ordering in the TEM sample of DLM1.2.

Despite the ordering of particles in the TEM micrographs, other typical behaviour of system DLM1.2 can also be observed on the same TEM sample. In figure 4.4 it is seen that on another region of the same TEM sample, the particles are more polydisperse and (possibly due to low concentration) do not show ordering.

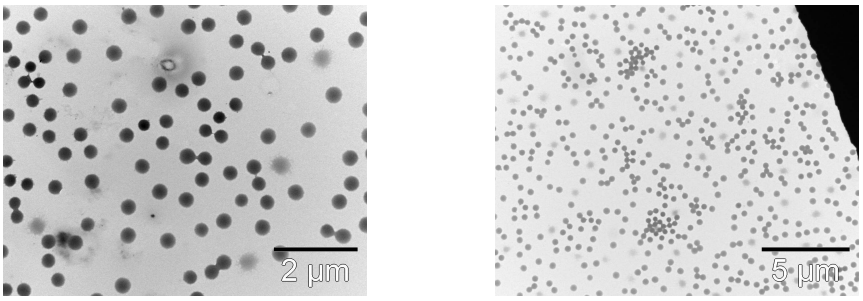

Figure 4.4: TEM micrographs of DLM1.2 revealing polydispersity in the TEM sample of DLM1.2, which might originate from drying effects, but can also be an indication for intrinsic polydispersity in the system.

Furthermore, upon even further analysis of the TEM results of DLM1.2 particles are found with a structural inconsistent outer region, as depicted in figure 4.5. It is known that the outer layer of pNipam is less crosslinked. Possibly, the inconsistent layer is the less crosslinked shell. It is, however, the question why not all particles on the TEM sample have this layer. This could mean that a part of the particles have met other conditions during the drying process. Another possibility is the presence of particles with different properties during the synthesis.

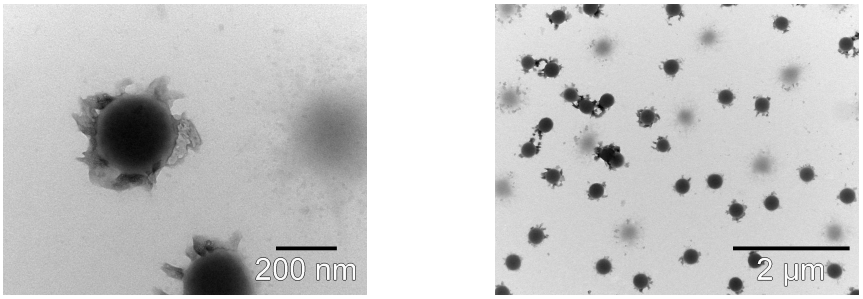

Figure 4.5: TEM micrographs of DLM1.2 revealing structural inconsitencies on the outside of the particles.

Since the effect of heating and drying cannot be neglected, it is hard to use TEM to be conclusive about the particles. It is clear that particles have formed, which display a variety of appearances. However, all the structural anomalies which are observed, might just as well not be an intrinsic property of the system. TEM proves the presence of particles and the results of the light scattering techniques give that the order of magnitude of the particles is around 650 nm. This is to small to be used in confocal microscopy, so alternative preparation methods have to be used to prepare the desired system.

4.1.2 PNipam-co-AAc microgel synthesis

Several preparations of pNipam-co-AAc have been performed based upon the protocol described in section 3.3.3. During these syntheses the observations were comparable to those of normal pNipam synthesis, except for the faster increase in turbidity. In these reactions, turbidity started to increases within 3 minutes of initiation. Furthermore, a kind of destabilisation took place, because solid material was observed on the stirring bar after the reaction. This is probably due to nucleation preferentially taking place on a relatively rough surface. DLM15.1 and DLM15.2 behaved in a similar way, so it is assumed that DLM15.1 is representative for DLM15.2. For this reason only results of DLM15.1 are discussed. The results of DLM35-DLM39 (also pNipam-co-AAc preparations), will be discussed later.

The forward scattering DLS measurements of DLM15.1 are displayed in figure 4.6, compared to the the forward measurements of DLM1.2. Also it is clear that the incorporation influences the LCST, since the co-AAc particles are not at their minimum diameter at 35 °C, whereas the normal pNipam particles are.

From the TEM micrographs (figure 4.7) it is clear DLM15.1 resulted in relatively monodisperse particles. The relative large size compared to DLM1.2 can also be noted from TEM. The same shell-like inconsistency as observed with system DLM1.2 is observed. Again, this might be due to the core-shell structure, as well as due to drying effects.

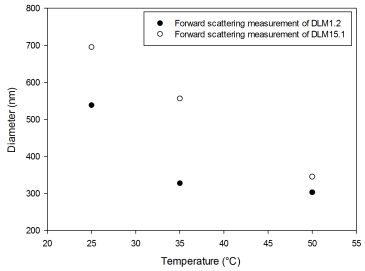

Figure 4.6: Average diameters from DLS measurements of DLM15.1, compared to the results of DLM1.2.

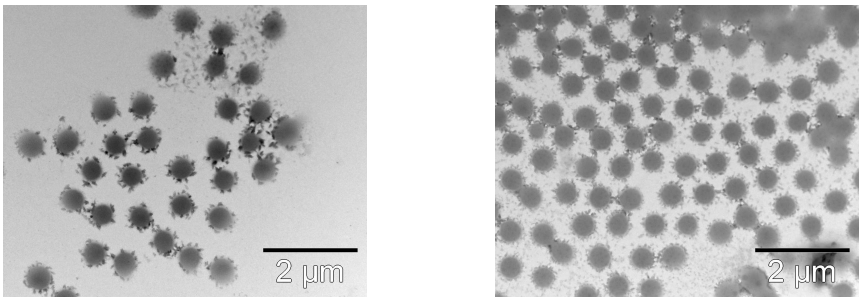

Figure 4.7: TEM micrographs of DLM15.1, a pNipam-co-AAc system.

4.2 NBD-MAEM-dyed microgel synthesis

Since the preparation of normal pNipam and pNipam-co-AAc is successful, the protocols seem suitable to prepare dyed microgel particles. In this section, all the preparations with NBD-MAEM as dye will be discussed. A full list of all the syntheses with dye is shown in table 3.2.

4.2.1 Dye synthesis

For the preparation of pNipam-co-NBD-MAEM systems, NBD-MAEM had to be synthesized. The first synthesis step in dye synthesis was the preparation of NBD-MAE, which is a straightforward reaction. Only one attempt was needed to produce this material. In the second step, NBD-MAE was converted into NBD-MAEM in a single reaction. At first, this reaction was not successful, due to the use of aged methacryloyl chloride. This material is highly reactive with water, and therefore unstable when not kept water-free. Furthermore, it polymerizes over time, making it unusable. The polymerization is indicated by the clear, colourless material turning brown.

Even though solubility of NBD-MAE in toluene is poor, it was readily converted to NBD-MAEM when using pure methacryloyl chloride. This is due to the fact that NBD-MAEM does have a good solubility in toluene, pulling the reaction towards product formation. After several attempts, NBD-MAEM was obtained. It has been used unpurified in the first few reactions. Afterwards, it has been purified by column chromatography and analyzed by means of ^{1}H and ^{13}C NMR spectroscopy to confirm purity. The obtained spectra can be found in appendix A.

4.2.2 PNipam-coNBD-MAEM preparations

After the successful preparation of a suitable dye, the synthesis of fluorescent particles was performed. The dye has a polymerizable group, which participates in the emulsion polymerization reaction. Therefore, dye is added before or during the reaction without further adaption of the reaction protocol (as described in section 3.3.4). Although it was already observed that pure crosslinked pNipam systems did not yield particles of 1 µm, no AAc is added, to keep the first synthesis as simple as possible. During all the reactions, an expected increase in turbidity was observed within 5 minutes of initiator addition. However, upon cooling, opacity decreased, to a much greater extent than was observed with normal pNipam microgels. This might be an indication that the polymer networks are crosslinked less densely.

To elucidate the observed phenomenon, the behaviour of the systems after the reaction was studied. Upon reheating the reaction mixture, an increase in turbidity was observed as well as precipitation large

aggregates. The aggregates did slowly dissolve again upon cooling. The formation of large precipitates was not observed during the reaction itself, indicating that irreversible changes took place after the reaction.

Both SLS and DLS were performed on diluted samples of the reaction mixtures. The results of these measurements were very incosistent and pointed towards an absence of particles. For this reason, TEM was used to obtain information about the systems. In figure 4.8 some typical micrographs of the attempted preparations are depicted. As can be seen, none of the systems yielded well-defined particles, since spherical consistent structures are absent. System DLM3.2 has some particles, but also a lot of loose polymer. With all the other samples, loose polymer aggregates or large droplike structures is the only thing that is observed.

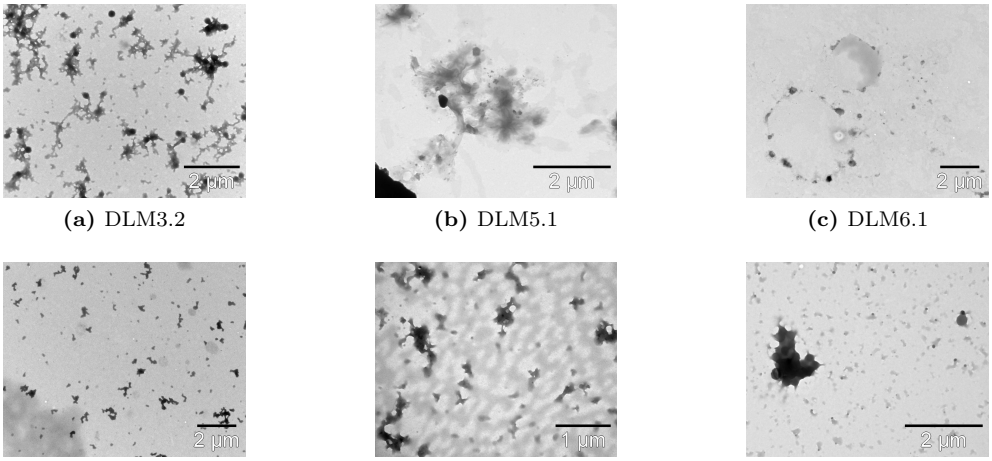

(a) DLM3.2 **(b)** DLM5.1 **(c)** DLM6.1

(d) DLM7.1 **(e)** DLM8.1 **(f)** DLM9.1

Figure 4.8: TEM micrographs of the first attempts to produce pNipam-co-NBD-MAEM systems.

Irreversible thermal behaviour of dyed systems

Due to the observed behaviour of the systems' turbidity and precipitate, it was thought that the system changed irreversibly upon cooling the reaction mixture. Therefore, DLM9.2 was synthesized for an attempt to make *in situ* TEM sample of the reaction mixture. To achieve this, the system was synthesized according to the protocol described in 3.3.4. During this synthesis, a sample of hot reaction mixture was taken with a hot pasteur pipette and diluted in hot (60 °C) milliQ water. Then, a TEM sample was prepared (according to section 3.4.1) on a heated TEM-grid. The grid was only allowed to cool when it was entirely dry. This way it was attempted to make a *in situ* TEM sample of the reaction mixture. The TEM results of this sample were compared with a "normal" sample from DLM9.2, which was diluted in water of room temperature. The results are depicted in figure 4.9. The difference between both samples is very clear. The normally prepared sample reveals formation of a lot of polymer aggregates, but no particles. The *in situ* sample reveals formation of particles. For this reason it is justified to say that cooling down the reaction mixture induces an irreversible change of the system.

This behaviour again points in the direction of a low content of crosslinking. The mechanism behind the observed phenomena might be explained as follows. At high temperature the particles are in a shrunken compact state, although poorly crosslinked. Upon cooling, the particle takes up large amounts of water and swells. As a result, the chains might protrude from the surface, possibly interpenetrating with chains from other poorly crosslinked particles, forming a network. In principle the protruding chains should sterically stabilize the particles. Why this is not the case, is hard to elucidate. The described mechanism is depicted schematically in figure 4.10. The precipitative behaviour of the systems upon reheating can now also be explained. When the LCST is reached, the dissolved polymer network is not soluble anymore and precipitates. Instead of forming smaller particles, large aggregates are formed, since their chains are interpenetrated.

The synthesis of pNipam-co-NBD-MAEM has so far been problematic. The cause for the problems lies in the addition of dye, since the synthesis works fine without NBD-MAEM. Possible explanations are impure dye, intrinsic properties of the dye or the effect of organic solvents. All three possible reasons will be discussed.

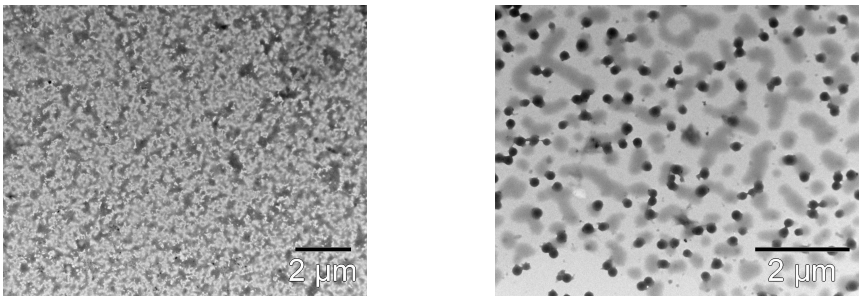

(a) **(b)**

Figure 4.9: TEM micrographs of DLM9.2: **(a)** At the sample prepared at room temperature only polymer is observed. **(b)** At the hot reaction mixture sample, not cooled before drying, distinct particles can be observed.

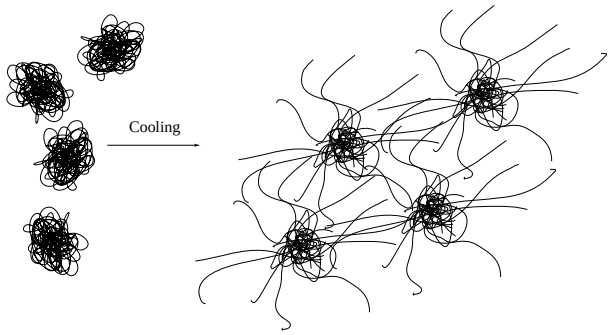

Figure 4.10: Schematic depiction of a process in which particles interpenetrate semi-irreversible upon cooling, in case of bad crosslinking. This way a polymer network is formed.

Since NBD-MAEM was not obtained from a commercial supplier, impurities can be expected. Indeed, the first of the pNipam-co-dye syntheses have been performed with impure dye as was confirmed later with ^{1}H NMR spectroscopy. However, upon purification and characterization, the results did not improve. For this reason it is assumed that the impurities in the dye were not the main cause of the problems. Another possibility is that the reaction rates of the different monomers differ a lot. For instance, if NBD-MAEM reacts significantly faster with the crosslinker than Nipam, small dye-crosslinker particles will be formed without Nipam. The remaining Nipam will then form long, uncrosslinked polymer chains which easily dissolve upon cooling and will not return to a microscopic globular state anymore. Another possible explanation might be the influence of the charge which is present on the dye. Although the net charge of the molecule is zero, it does have one positive and one negative charge. This might have influence on the incorporation of the dye. In an attempt to lower the negative influence of the NBD-MAEM on the reaction course, addition in portions has been tried (with DLM3.2, DLM5.1, DLM6.1, DLM7.1, DLM8.1 and DLM9.1). In this procedure, a small amount of dissolved dye was added before initiation, with more dye being added at regular intervals in the first part of the reaction. In this way, the concentration of dye throughout the reaction should be lower, since the dye is expected to be consumed before a new portion is added. However, since this was already applied to nearly every failed synthesis, this is apparently not the only factor.

The role of dye solvents

To produce dyed particles, the dye needs to be added to the reaction mixture. Because both dyes used are poorly soluble in water, organic solvents had to be used, which might have an influence on the course of the reaction. To test this influence, three pNipam-co-AAc particle synthesis have been performed with the addition of toluene, butanol and ethanol. The syntheses were done as described in section 3.3.3, with the solvent being added just before initiation. The amounts of the added solvents depended on the solubility of the dyes in the solvents and are listed in table 4.2.

The syntheses of pNipam-co-AAc particles with addition of organic solvents did all yield particles, although differences were observed. In figure 4.12 the TEM micrographs of the reaction mixtures are

Table 4.2: Amounts of solvents used in three pNipam-co-AAc syntheses

Batch label	Solvents	Volume (mL)
DLM37	Toluene	1.0
DLM38	Butanol	1.0
DLM39	Ethanol	2.0

shown. In the case of toluene, bubble-like structures, a lot larger than the particles, were observed. Toluene is, unlike ethanol and butanol, insoluble in water. Possibly, the equilibrium between Nipam in aqueous solution and Nipam in micelles gets disturbed by the addition of toluene. Nipam might act as a surfactant, stabilizing small droplets of toluene. Upon initiation, the Nipam gets polymerized, producing the shell-like structures observed on TEM. For ethanol and butanol the effect is less pronounced, but low-contrast structures can be observed. This indicates that also these two solvents influence the reaction.

To see if there are differences in size and thermoresponsive behaviour, DLS has been performed, as shown in figure 4.11. There are some differences in size, but they are not large enough to relate to the used solvent.

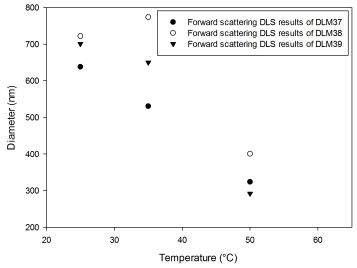

Figure 4.11: Thermal response characterization by means of DLS of DLM37, DLM38 and DLM39.

Since most organic solvents are volatile, it might be possible to remove the solvent by a flow of nitrogen. To confirm this, toluene was added long before addition of initiator. The flow of nitrogen was increased for an hour in order to possibly remove most (or all) of the toluene. After this synthesis, the shell-like structures were not observed with TEM. However, the synthesis was performed without AAc (unlike the solvent tests with DLM37, DLM38 and DLM39). So either the AAc plays a crucial role, or it is indeed possible to evaporate the toluene by means of heating and appliance of a nitrogen flow. The latter hypothesis is supported by the fact that the odor of toluene was not noticeable anymore, indicating that at least the most of the toluene indeed evaporated. The other solvents have not been tested in this way.

4.2.3 High crosslinker/initiator pNipam-co-NBD-MAEM preparations

To achieve the goal of synthesising fluorescent pNipam particles, other synthesis procedures were tried. Rianne Plantenga, who also worked on pNipam microgels, presented her preparation method in which the concentrations of all reactants (Nipam, BIS and initiator) were significantly higher than in the previously performed syntheses. Especially the high amount of charge, in the form of KPS, might be able to stabilize

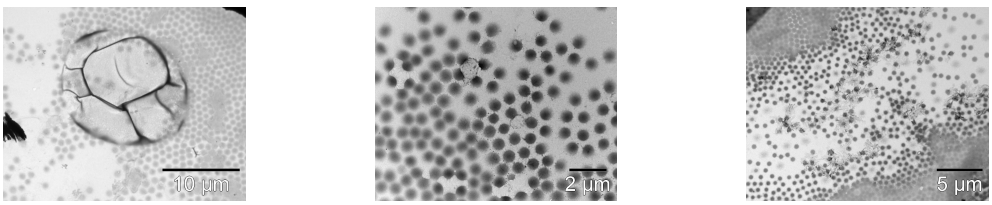

(a) DLM37 **(b)** DLM38 **(c)** DLM39

Figure 4.12: TEM micrographs of the preparation of pNipam-co-AAc in the presence of organic solvents. Especially the vesicle-like structures in the co-toluene synthesis are striking.

the particles during synthesis. Therefore, a single co-NBD-MAEM synthesis was performed using the relatively high concentrations of crosslinker and initiator. During the reaction, a turbidity increase was observed 3 minutes after initiation, indicating particle formation. However, a tendency to aggregate was also observed. Although this indicates that the (seed) particles are not stable during the reaction, it is in principle possible to remove the aggregation by filtration afterwards.

The TEM micrographs of DLM17.1 are shown in figure 4.13. The open internal structure of the particles might indicate low crosslinking. It might however also be a drying effect. Also, the origin of the small black points in the particles is unclear. It might be small particles of dye/crosslinker. Another notable effect is the 2D ordering. This was also observed with DLM1.2, although the interparticle distance is larger with DLM17.1. This is due to higher charge or higher steric repulsion.

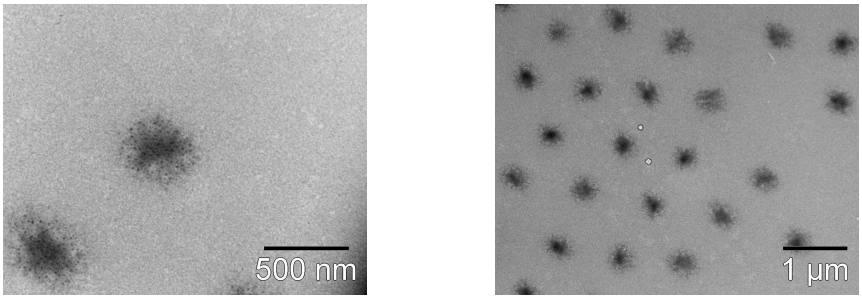

(a) **(b)**

Figure 4.13: TEM micrographs of DLM17.1 **(a)** revealing the internal structure of the particles. The open structure and black dots are remarkable. **(b)** Revealing the 2D ordering.

Size-temperature dependence has been explored using DLS, as shown in figure 4.14. It is immediatly clear that the particles are very small, having a diameter of only about 400 nm at room temperature. Additionally, the estimated value for R_g, as obtained by SLS, was 372 nm.

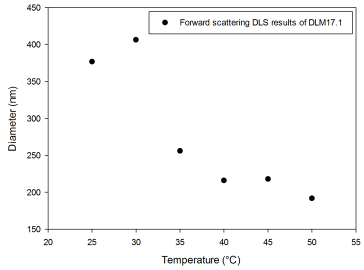

Figure 4.14: DLS-obtained size-temperature dependence of DLM17.1.

Confocal microscopy micrographs of DLM17.1 can be foun in figure 4.15. Since the particles are visible, it is clear that the dye is incorporated in sufficient amounts. However, the estimated interparticle distances are below 1.0 µm, making the system unsuitable for the desired experiment, as was already shown with DLS.

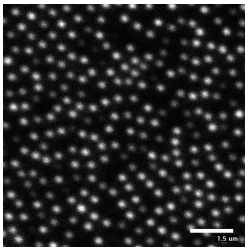

Figure 4.15: Confocal microscopy micrographs of DLM17.1. Typical sizes are far less than 1 µm.

It can be concluded that the synthesis protocol of section 3.3.5 is more successful for preparing

fluorescent pNipam particles than the protocol of section 3.3.4. Regrettably, the particles created in the process do not have the desired dimensions of about 1.0 µm.

4.2.4 PNipam-co-AAc-co-NBD-MAEM preparations

Another way to to produce fluorescent pNipam particles is with the incorporation of AAc. It was already known from previous experiments that particles copolymerized with AAc should have a size of around 1.0 µm at room temperature. With incorporation of AAc one introduces a pH-dependence of the amount of charge on the particles.

Preparations of pNipam-co-AAc in presence of dye have been performed, based upon the protocol described in section 3.3.6. During all these preparations, the mixture became turbid within 3 minutes of reaction initiation. Upon cooling, the turbidity decreased a lot again, which could be caused by swelling or dissolution of polymer. As opposed to the regular pNipam-co-NBD-MAEM, the increase in turbidity was not accompanied by precipitation upon reheating. This indicates that crosslinked particles were present and stable at room temperature. However, as with normal pNipam-co-AAc, a small amount of solid material was observed on the stirring bar after every synthesis.

The TEM micrographs of DLM16.1 are shown in figure 4.16. Again, the structural properties of the particles is hard to explain. The particles have a very open structure and seem to be interpenetrated. Although the former observation might indicate bad crosslinking, it is also possible that both effects are due to drying effects.

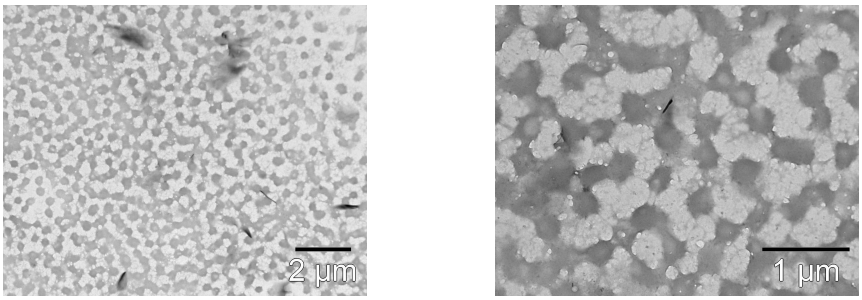

Figure 4.16: TEM micrographs of DLM16.1. The open structure of the particles is notable. Furthermore, the particles seem to have interpenetrated.

Again, DLS was performed, as shown in figure 4.17. It can be seen that the R_H is around 700 nm at room temperature. The fact that consistent DLS results are obtainable, again proves the formation of particles. Furthermore, the size is going towards the desired order of magnitude.

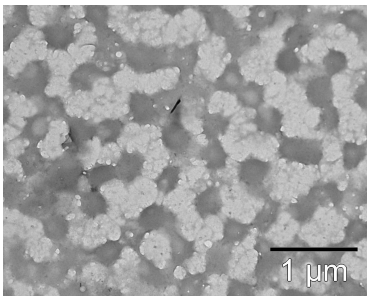

Figure 4.17: DLS-obtained size-temperature dependence of DLM16.

4.2.5 PNipam-co-NBD-MAEM preparations in acetate buffer

A few preparations of fluorescent pNipam microgels have been carried out in an acetate buffer according to the protocol described in section 3.3.7. A turbidity increase after 5 minutes was observed in all cases, again indicating particle formation. However, a lot of flocculation was also be observed during the reaction. One system did yield particles (DLM12.1), but an attempt to reproduce the synthesis did fail (DLM18.1), as was confirmed with TEM. During the reactions of these systems, a lot of flocculation was observed in all cases.

TEM micrographs for DLM12.1 are shown in figure 4.18 and reveal very high polydispersity. Also, some aggregated secundary nucleation van be observed. Again, drying effects might be the cause of these effects, especially the polydispersity.

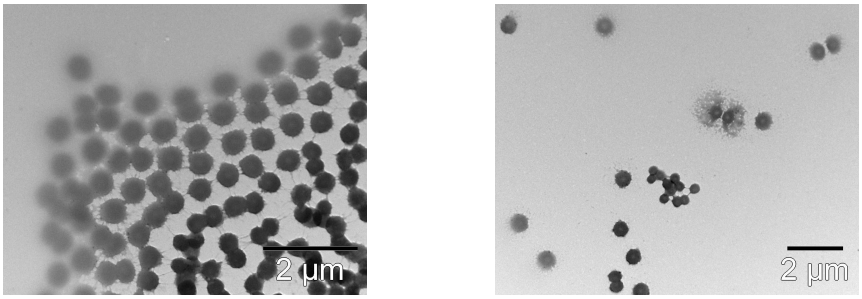

Figure 4.18: TEM micrographs of system DLM12.1.

A typical confocal microscopy micrograph can be found in figure 4.19 again revealing the high polydispersity. This probabably means that the observed polydispersity in TEM was no (or not exclusively) a drying effect in this case.

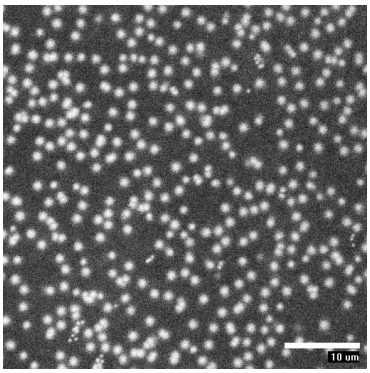

Figure 4.19: Confocal microscopy images of system DLM12.1. It is again clear that the system is very polydisperse.

To obtain more information about the size, DLS was used, as shown in figure 4.20. The particles are about 700 nm at room temperature, and 500 nm at elevated temperature. However, since the system is very polydisperse, it is questionable if the results of DLS can be used, since the fitting methods used need to be more complex then.

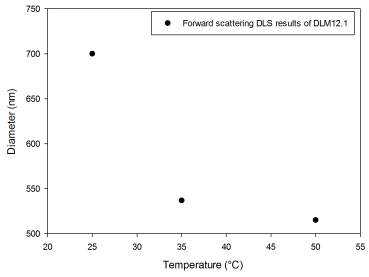

Figure 4.20: DLS-obtained size-temperature dependence of DLM12.1.

4.3 PolyFluor 570-incorporated microgel synthesis

Since synthesis of dyed particles based upon NBD-MAEM appeared to be difficult, PolyFluor 570 was used. The same functional group is present, so the principle of incorporation of this dye is the same as that of NBD-MAEM. A list of all the performed preparations can be found in table 3.2.

4.3.1 PNipam-co-PolyFluor 570 preparations in acetate buffer

Since the addition of buffer was one of the particle-yielding protocols in the NBD-MAEM-dyed preparations, this method was repeated once. The course of the reaction was the same as with the previous dye. Turbidity started increasing after 5 minutes again. Some flocculation was observed, although to a lesser extent than with NBD-MAEM. Furthermore, the dispersion could be seperated from the flocs by means of decantation or filtration.

In figure 4.21 the TEM micrographs obtained from a sample of DLM32 are shown. From these pictures it becomes clear that particle formation was successful during synthesis. However, it is also notable that the particles look very polydispers on the TEM sample. This might, however, be attributed to drying effects. This is especially plausible because the isolated particles are larger than the aggregated particles.

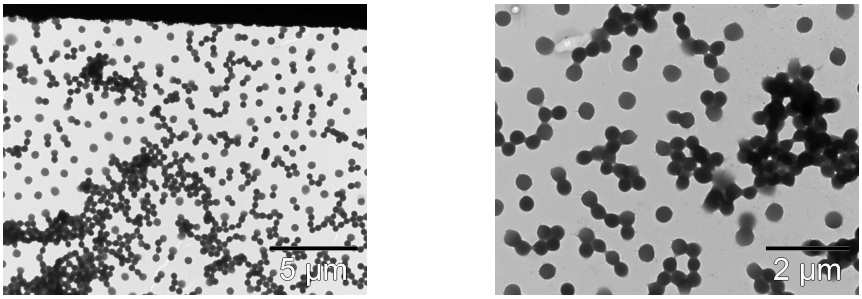

Figure 4.21: TEM micrographs from system DLM32.

The thermal response of DLM32 was characterized by means of DLS. These measurements have been performed in pure water and in buffer with pH around 4.0. The resulting graphs of the diameter can be found in figure 4.22. It is clear that the pH does not influence the LCST, as would be expected for pure pNipam. Since the particles are smaller, the diameter of the particles is affected, but this is not due to pH, but due to ionic strength. A higher ionic strength is capable of screening the repulsion between the negative charges on the pNipam particles, allowing it to more easily contract. SLS has also been performed at room temperature, resulting in a R_g of about 1050 nm.

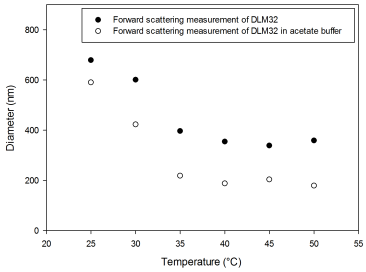

Figure 4.22: Diameter calculated from forward scattering DLS results for system DLM32 in milliQ water and in buffer (pH=4).

Confocal microscopy

A sample of DLM32 (with concentration the same as the reaction mixture), has been looked at by means of confocal microscopy (figure 4.23). The typical distances between the particles are about 1.0 µm. This order of magnitude is confirmed by SLS. The results of DLS show a R_H of around 700 nm, but this can be accounted for by the property of pNipam particles, since water can move relatively freely through their shell.

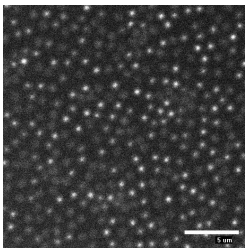

Figure 4.23: A confocal microscopy micrograph of a sample of DLM32. The typical interparticle distances are around 1 µm.

4.3.2 PNipam-co-AAc-co-PolyFluor 570 preparations

Fluorescent pNipam-co-AAc syntheses looked promising enough to try again with another dye. Therefore, this preparation has been repeated several times with attempted incorporation of PolyFluor 570. In all the attempts, the reaction mixture turned turbid within 4 minutes. However, as with all the previous pNipam-co-AAc preparations, flocculation at the stirring bar was again observed. No notable deviations during the course of reaction were observed for any of the preparations. The same holds for the characterization. For this reason, the results for DLM29 will be discussed here, which are representative for the other batches.

TEM micrographs of DLM29 are depicted in figure 4.24. The micrographs proof the formation of particles. However, no other conclusions can be drawn from the images. Both the apparent polydispersity and large size might be accounted for by drying effects.

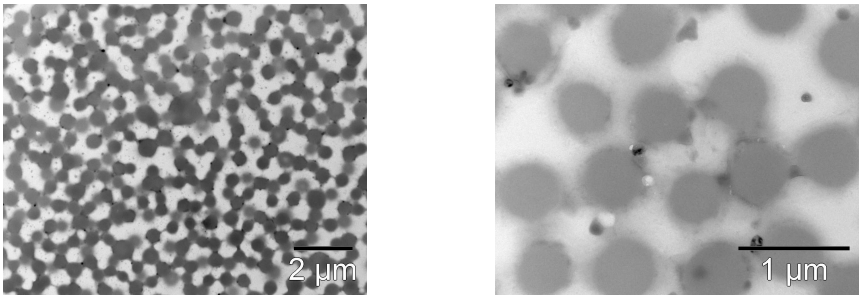

Figure 4.24: TEM micrographs of a sample of DLM29.

The diameter-temperature plot obtained by using DLS (figure 4.25) reveals the thermoresponsive behaviour. It can be seen that the particles are not larger than 1.0 µm. At 25 °C the measured diameter is lower than at 30 °C, which is probably due to a measurement error. At 25 °C, problems have been observed more often with DLS, since scattering is the lowest then, due to a relative small refractive index difference between particles and solvent.

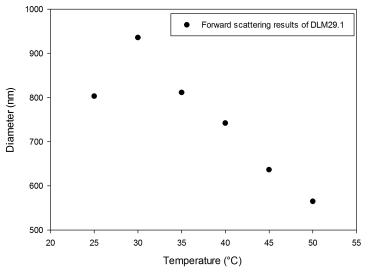

Figure 4.25: Diameter-temperature plot of DLM29, revealing size information and thermoresponsive behaviour.

Confocal microscopy imaging has been performed on system DLM29 (figure 4.26). Although DLS showed that the particles are probably not larger than 1.0 µm, the interparticle distance in these images is about 1.5 µm. This high interparticle distance is probably due to charge and steric repulsion. For this reason, crystals are formed (as can be seen in figure 4.26 (b)), despite the polydispersity of the system.

When the ionic strength is increased (by using a buffer or adding salt), polydispersity will cause the system to form a glass state instead of crystals.

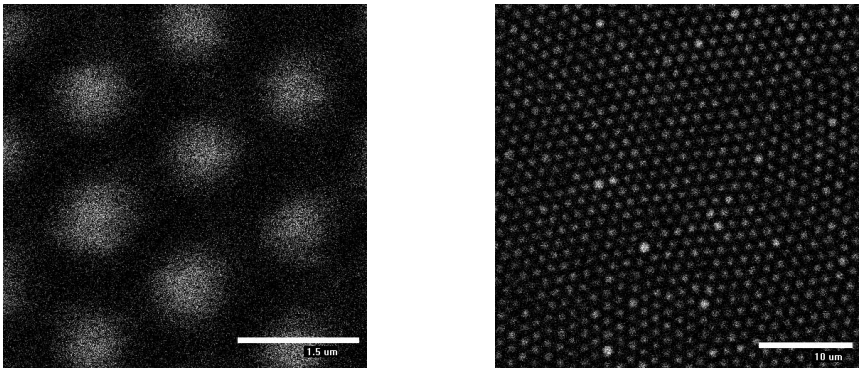

(a) **(b)**

Figure 4.26: Micrographs of confocal microscopy measurements of DLM29 are depicted. **(a)** A close-up of the sample, showing an interparticle distance of about 1.5 µm. **(b)** An overview of the sample, showing crystalline behaviour and revealing the polydispersity of the system.

4.3.3 High crosslinker/initiator pNipam-co-PolyFluor 570 preparations

Although it was highly probable that a repeat of a synthesis with high crosslinker and initiator amounts would yield small particles again, the protocol was repeated, to see if the results were indeed comparable to their co-NBD-MAEM counterpart (figure 4.13). During the synthesis the turbidity increase was observed after 3 minutes. Again, a drop in turbidity was observed upon cooling. As with DLM17, flocculation was again observed during the reaction, which indicates that the particles still are not stable during the reaction.

TEM images of DLM26 in figure 4.27 reveal the small dimensions of the particles. Since the synthesis protocol of DLM17 and DLM26 only differ in the choice of dye, the TEM pictures can be compared. The structure of DLM17 on TEM is entirely different than that of DLM26, with DLM17's particles having a far more open structure. Although this difference might be again explained by drying effects, it is peculiar that an almost exact repeat of synthesis yields such a large difference in TEM images.

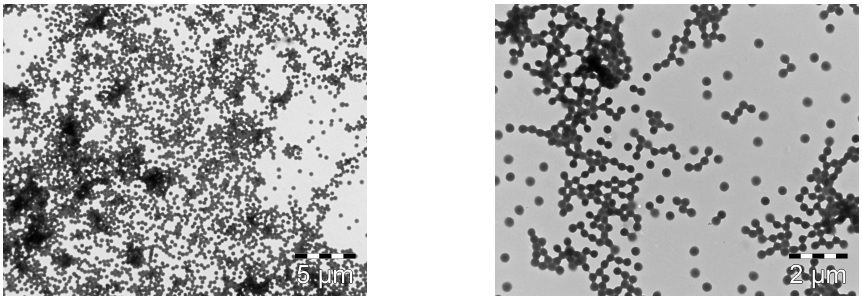

(a) **(b)**

Figure 4.27: TEM micrographs of DLM26 showing an overview of the sample (**(a)**) and a close-up **(b)**.

The Zetasizer results of DLM26 (figure 4.28) indicate that system DLM26 consists of somewhat larger particles, with a diameter of about 600 nm at lower temperature, shrinking to a diameter of about 350 nm at elevated temperature. This information is supported by the data obtained using SLS, which gives a R_g of about 550 nm at room temperature.

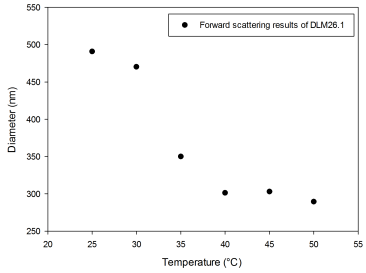

Figure 4.28: Zetasizer DLS results which shows the thermoresponsive behaviour of DLM26 for a forward scattering measurement.

The confocal images of DLM26 (figure 4.29) reveal a high degree of ordering, both hexagonal, as well as squarelike. This ordering was only 2D, and might be templated by the glass surface. The large interparticle distance is striking. It can probably not originate from charge repulsion alone, since associated Debeye lengths are hard to achieve in water. Possibly, the particles have long polymer "hairs", which keep the particles seperated due to steric repulsion.

Influence of reaction temperature on pNipam synthesis

It is known that reaction temperature has an influence on polydispersity and size. In general, at lower temperatures (but still far above the LCST), the formed particles are bigger.[30] When using the high concentration initiator/crosslinker approach, some lower temperature syntheses have been performed. It was observed that the particles produced at lower temperature (60˚) were larger than those produced at the normal reaction temperature of (70˚), as shown in figure 4.30.

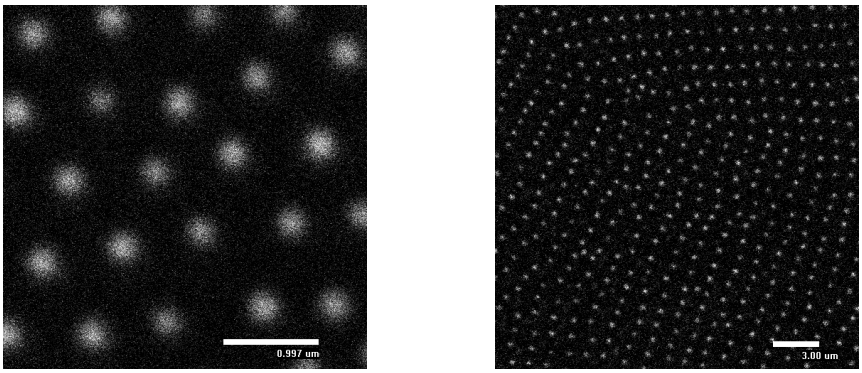

(a) **(b)**

Figure 4.29: Confocal images of **(a)** a close-up of system DLM26 in a hexagonal arrangement **(b)** an overview picture of system DLM26 in a square-like arrangement.

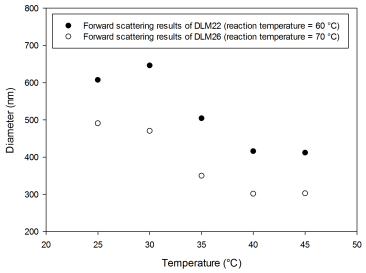

Figure 4.30: Diameter-temperature dependence curves of DLM22 and DLM26, obtained using DLS. Size differences originating from a different reaction temperature can clearly be observed.

Chapter 5

Conclusions and outlook

The ultimate goal of the project was the synthesis of two complementary pNipam microgel systems. The two systems had to be stable, fluorescent (at different wavelengths), and be in the same order of magnitude (about 1.0 µm). Many preparations have been performed, trying to make the desired systems. The simplest synthesis protocol, dyed regular pNipam, seems unsuitable for the preparation of fluorescent particles, since no particles were formed. According to our synthesis results, the protocol in which more crosslinker and initiator is used is also unsuitable for a successful synthesis of stable pNipam microgels, because of the formation of aggregation. Furthermore, the size of the particles is below the desired 1000 nm. The copolymerisation with AAc shows to be a promising way of creating fluorescent pNipam systems. The particles created in this synthesis are in the order of diameter of 1.0 µm, which is the desired size. However, all the systems are rather polydisperse, making them unsuitable for controlled crystallization. The synthesis of fluorescent pNipam in acetate buffer also shows to be a promising method. The particles obtained in this way are between 0.75 and 1.0 µm and their polydispersity seems to be low.

During the research described in this thesis, the quality of the prepared systems kept increasing. Possibly, by doing some minor adaptions, the used protocols are viable ways to create well-defined pNipam systems. It is eligible for research of colloidal crystals and defects to invest some more time in the perfection of these protocols. When it is possible to create several pNipam systems, all with their own, distinct properties, the experiment described in this thesis probably is not the only interesting possibility. Improvement of the used protocols is described in the following subsections.

The demonstrated preparations of pNipam-co-AAc yielded the largest particles. However, the high polydispersity disqualifies the systems from being suitable in crystal studies. Possibly the polydispersity will become lower by using lower reaction temperatures, since growth is slowed down. Although the particles created in acetate buffer are not as big as the pNipam-co-AAc particles, this method also is a promising one. Especially the apparently low polydispersity on confocal microscopy micrographs makes the synthesized system interesting. However, to use the particles in defect diffusion studies, their size should be larger. One way to achieve this, might be to repeat the synthesis on a lower temperature (around 60 °C). Another way to try increase size might be to add more Nipam in the course of the reaction. Assuming that most of the initiator is already incorporated in particles, no new seeds will be created, which means that the Nipam will be consumed by the existing particles, making them larger.

Since some stable systems have been prepared, their properties can be further analyzed with light scattering and microscopy techniques. On the first place, more information about the systems might lead to possible improvements of the synthesis protocols. Better defined systems will increase the feasibility of the experiment. Also, upon further characterization, possible imperfections of the systems can be identified. This knowledge can de used to adapt the final experiment.

Chapter 6

Acknowledgements

During this research I have had a lot of help and support and I want to thank all who were involved. First of all, I thank Janne-Mieke for being my daily supervisor. Without her input and help, I would not have come so far in this research as I have now. Also Andrei and the crystal club are thanked for usefull discussions (togethere with truckloads of candy). I am also very grateful to Jan. Without him sharing his experience on pNipam and confocal microscopy, I would not have a report so full of syntheses and pictures. For help with the SLS and the DLS, I am grateful to Emile en Bonny. For the organic knowledge needed to produce my dye I want to thank Timo and Vital. I thank all the students who have been in the master student room during may stay. Although I am the person having problems concentrating, they all had to suffer just as much. For me, procrastination is not done in silence. Finally, I would like to thank all members of the FCC group. I really enjoyed my stay here.

Bibliography

[1] H. G. Bueren. *Imperfections in crystals*. North-Holland Publishing Company, 2nd revised edition, 1961.

[2] D. Hull and D. J. Bacon. *Introduction to dislocations*. Elsevier Ltd., 4rd edition, 2001.

[3] R. S. Muller, I. K. Theodore, and M. Chan. *Device electronics for integrated circuits*. Wiley, 3rd edition, 2002.

[4] K. Arakawa, K. Ono, M. Isshiki, K. Mimura, M. Uchikoshi, and H. Mori. Observation of the one-dimensional diffusion of nanometer-sized dislocation loops. *Science*, 318:956–959, 2007.

[5] Y. Matsukawa and S. J. Zinkle. One-dimensional fast migration of vacancy clusters in metals. *Science*, 318(5852):959–62, 2007.

[6] W. Lechner and C. Dellago. Defect interactions in two-dimensional colloidal crystals: vacancy and interstitial strings. *Soft Matter*, 5(14):2752, 2009.

[7] D. H. Everett. *Basic Principles of Colloid Science*. The royal society of chemistry, 1st edition, 1988.

[8] P. N. Pusey and W. van Megen. Phase behaviour of concentrated suspensions of nearly hard colloidal spheres. *Nature*, 320:340–342, 1986.

[9] P. Jiang, J. F. Bertone, K. S. Hwang, and V. L. Colvin. Single-Crystal Colloidal Multilayers of Controlled Thickness. *Chemistry of Materials*, 11(8):2132–2140, 1999.

[10] A. van Blaaderen, R. Ruel, and P. Wiltzius. Template-directed colloidal crystallization. *Science*, 385:321–324, 1997.

[11] P. Schall, I. Cohen, D. A. Weitz, and F. Spaepen. Visualization of dislocation dynamics in colloidal crystals. *Science*, 305(5692):1944–8, 2004.

[12] J. M. Meijer, V. W. A. De Villeneuve, and A. V. Petukhov. In-plane stacking disorder in polydisperse hard sphere crystals. *Langmuir*, 23(7):3554–3560, 2007.

[13] A. Pertsinidis and X. S. Ling. Diffusion of point defects in two-dimensional colloidal crystals. *Nature*, 413(6852):147–50, 2001.

[14] J. Hilhorst, V. V. Abramova, A. Sinitskii, N. A. Sapoletova, K. S. Napolskii, A. E. Eliseev, D. V. Byelov, N. A. Grigoryeva, A. V. Vasilieva, W. G. Bouwman, K. Kvashnina, A. Snigirev, S. V. Grigoriev, and A. V. Petukhov. Double stacking faults in convectively assembled crystals of colloidal spheres. *Langmuir*, 25(17):10408–10412, 2009.

[15] R. H. Pelton and P. Chibante. Preparation of Aqueous Latices with N- Isopropylacrylamide. *Colloids and surfaces*, 20:247–256, 1986.

[16] R. H. Pelton. Temperature-sensitive aqueous microgels. *Advances in colloid and interface science*, 85(1):1–33, 2000.

[17] A. M. Alsayed, M. F. Islam, J. Zhang, P. J. Collings, and A. G. Yodh. Premelting at defects within bulk colloidal crystals. *Science*, 309:1207–1210, 2005.

[18] Y. Peng, Z. Wang, a. M. Alsayed, a. G. Yodh, and Y. Han. Melting of Colloidal Crystal Films. *Physical Review Letters*, 104(20):19–22, 2010.

[19] S. B. Debord and L. A. Lyon. Influence of Particle Volume Fraction on Packing in Responsive Hydrogel Colloidal Crystals. *Journal of Physical Chemistry B*, 107(13):2927–2932, 2003.

[20] C. D. Jones and L. A. Lyon. Synthesis and Characterization of Multiresponsive Core-Shell Microgels. *Macromolecules*, 33(22):8301–8306, 2000.

[21] B. J. Alder and T. E. Wainwright. Phase Transition for a Hard Sphere System. *The Journal of Chemical Physics*, 27(5):1208, 1957.

[22] P. N. Pusey, E. Zaccarelli, C. Valeriani, E. Sanz, W. C. K. Poon, and M. E. Cates. Hard spheres: crystallization and glass formation. *Philosophical transactions. Series A, Mathematical, physical, and engineering sciences*, 367(1909):4993–5011, 2009.

[23] G. S. Whitby and M. Katz. Synthetic Rubber (Concluded). *Industrial and Engineering Chemistry*, 25(12):1338–1348, 1933.

[24] W. V. Smith and R. H. Ewart. Kinetics of Emulsion Polymerization. *The Journal of Chemical Physics*, 16(6):592–599, 1948.

[25] X. Wu. The kinetics of poly(N-isopropylacrylamide) microgel latex formation. *Colloid & Polymer Science*, 272(4):467–477, 1994.

[26] R. Acciaro, T. Gilányi, and I. Varga. Preparation of monodisperse poly(N-isopropylacrylamide) microgel particles with homogenous cross-link density distribution. *Langmuir*, 27(12):7917–7925, 2011.

[27] M. Stieger, W. Richtering, J. S. Pedersen, and P. Lindner. Small-angle neutron scattering study of structural changes in temperature sensitive microgel colloids. *The Journal of chemical physics*, 120(13):6197–6206, 2004.

[28] S. Meyer and W. Richtering. Influence of Polymerization Conditions on the Structure of Temperature-Sensitive Poly(N -isopropylacrylamide) Microgels. *Macromolecules*, 38(4):1517–1519, 2005.

[29] G. Bosma, C. Pathmamanoharan, E. H. A. de Hoog, W. K. Kegel, A. van Blaaderen, and H. N. W. Lekkerkerker. Preparation of monodisperse, fluorescent PMMA-latex colloids by dispersion polymerization. *Journal of colloid and interface science*, 245(2):292–300, 2002.

[30] J. Gao and B. J. Frisken. Influence of Reaction Conditions on the Synthesis of Self-Cross-Linked N-Isopropylacrylamide Microgels. *Langmuir*, 19(13):5217–5222, 2003.

Appendix A

NMR results